PERFORMANCE STUDY OF CATHODE CATALYST LAYER IN A PEM FUEL CELL USING AN AGGLOMERATE MODEL

A DISSERTATION

Submitted in the partial fulfillment of the

requirements for the award of the degree

of

INTEGRATED DUAL DEGREE

(Bachelor of Technology & Master of Technology)

in

CHEMICAL ENGINEERING

(With specialization in Hydrocarbon Engineering)

By

RAKTIM MITTRA

DEPARTMENT OF CHEMICAL ENGINEERING
INDIAN INSTITUTE OF TECHNOLOGY, ROORKEE
ROORKEE-247667
JUNE-2013

CANDIDATE'S DECLARATION

I hereby assure that the work entitled **"Performance study of cathode catalyst layer in a PEM fuel cell using an agglomerate model"** being presented in this dissertation report for the partial fulfillment of the award of **Integrated Dual Degree (Bachelor of Technology and Master of Technology)** in **Chemical Engineering** with specialization in **Hydrocarbon Engineering** is an authentic record of my own work carried out under the supervision of **Dr. Prakash Biswas,** Assistant Professor, Department of Chemical Engineering, Indian Institute of Technology Roorkee, Roorkee.

The matter presented in this report has not been submitted by me for the award of any other degree of this or any other institute.

Place: Roorkee Raktim Mittra

Date: Enrol. No: 08210014.

CERTIFICATE

This is to certify that above statement made by the candidate is correct to the best of my knowledge.

Prakash Biswas, PhD
Assistant Professor
Department of Chemical Engineering
Indian Institute of Technology Roorkee
Roorkee-247667, (India).

ACKNOWLEDGEMENTS

I am greatly indebted to my supervisor **Dr. Prakash Biswas**, Assistant Professor, Department of Chemical Engineering, Indian Institute of Technology Roorkee for his keen interest, constant guidance and encouragement for completion of this project report. His experience and deep insight of the subject held this work always on a smooth and steady course.

I am also thankful to Dr. Vijay Kumar Agarwal, Professor and Head, Department of Chemical Engineering, Indian Institute of Technology, Roorkee for providing various facilities during the course of this dissertation.

I also express my sincere gratitude to all well-wishers who in any manner directly or indirectly have put a helping hand in any part of this piece of work. Above all, I would like to thank my parents for their love, faith and support for me which has always been a constant source of inspiration.

Raktim Mittra

ABSTRACT

A comprehensive agglomerate model for the cathode catalyst layer (CCL) performance in a polymer electrolyte membrane fuel cell (PEMFC) has been developed. The overall transport phenomena and the electrochemical kinetics of each species namely oxygen, electrons and protons inside the CCL is considered in this model. The model is developed in such a way that it can be reduced to a pseudo-homogenous model when the agglomerate radius approaches zero. The validation of the model is done with the experimental results of Ticianelli et.al [39] .This is done by first estimating the value of agglomerate radius, ionomer film thickness and ionomer volume fraction for one set of operating conditions and then validating the model for another set of operating conditions. The agglomerate model is compared with pseudo-homogenous model. It is found that the pseudo-homogenous model over predicts the cell voltage, particularly at high current densities. The effect of two operational parameters namely operating temperature and oxygen pressure and five structural parameters namely agglomerate radius, ionomer film thickness, platinum loading, ionomer volume fraction and catalyst layer (CL) thickness on PEMFC performance is investigated. It is found that the increase in operating temperature and pressure improves the performance of PEMFC while the increase in agglomerate radius and ionomer film thickness has a negative influence on PEMFC performance. Optimum values of platinum loading and ionomer fraction is calculated for three overpotentials: 0.3, 0.6 and 0.9 V. The results show that the optimum platinum loading decreases while the optimum ionomer fraction increases with increase in overpotential. The utilization of the CL is found to decrease with increase in CL thickness.

TABLE OF CONTENTS

LIST OF FIGURES

LIST OF TABLES

CHAPTER-1
INTRODUCTION

1.1 Introduction

The explosion of human population in the last 100 years has made the conventional energy sources like fossil fuels to become increasingly inadequate for the needs of mankind. Scientists have incessantly voiced their concerns over global warming resulting from greenhouse emissions from carbon dioxide which is produced by the combustion of all fossil fuels. Both these issues make use of alternative energy sources more desirable in the present scenario. This has fueled the interest in the development of new technologies to harness energy from solar, wind, tidal and nuclear power in a more efficient manner.

In the last four decades, the interest in hydrogen energy in the scientific community as a solution to these global problems has seen an extraordinary surge. Hydrogen possesses many unique properties that make it particularly desirable as an energy carrier. Hydrogen is the lightest fuel on the planet. It has the highest calorific value (141, 790 kJ/kg) among all other fuels .With water as the only by-product, it provides the cleanest form of combustion. Further, the energy of hydrogen can be directly converted to electrical energy with higher efficiencies through electrochemical reactions. The device used to facilitate this energy conversion is called a fuel cell.

A fuel cell uses hydrogen as a fuel and oxygen as an oxidant to produce electrical energy with water and residual heat as the only by-products. Fuel cells and batteries are functionally similar to each other. But, while batteries store a fixed amount of reactants within itself, a fuel cell requires a continuous supply of reactants. A feature that makes fuel cells more desirable than conventional engines is that the efficiency of engines is limited by the Carnot efficiency. Since the fuel cells are electrochemical devices, this limitation do not apply to them. Typically, the efficiency of fuel cell ranges from 15-25% while the efficiency of fuel cell ranges from 40-60%. Hence, fuel cells are nearly three times more efficient than conventional engines. It is expected that fuel cells will completely replace conventional engines by the end of this century.

Various types of fuel cell are currently being developed. While some of them have been already commercialized, others are still in the research phase. These fuel cells are expected to find applications almost everywhere ranging from power plants to houses, cars, laptop batteries and mobile chargers.

The classification of fuel cells is done on the basis of choice of fuel, oxidant, electrolyte and the operating temperature range. The major types of fuel cells are as follows:

1. Polymer electrolyte membrane or Proton exchange membrane fuel cell (PEMFC).
2. Phosphoric acid fuel cells (PAFC).
3. Direct methanol fuel cell (DMFC).
4. Alkaline fuel cell (AFC).
5. Solid oxide fuel cell (SOFC).

Among these fuel cells, PEMFC has been reported as the most promising type of fuel cell. This is because the PEMFC has a high power density (0.7-1 W/cm^2), high efficiency (30-45%), easy scalability and low operating temperature (40-100^0C). Due to this reason, the modeling of PEMFC cathode is the focus of this thesis research.

1.2 PEMFC components

PEMFC was first used by NASA as a backup power source in its project Gemini space program in 1970 [1]. General Electric has continued to work on PEMFCs and employed them for all the future space programs [1]. Presently, Ballard power systems have been developing PEMFCs for a wide range of commercial purposes like vehicles, stationary power, laptop batteries etc.

A PEMFC comprises of a polymer membrane which is sandwiched between the cathode and anode. The polymer membrane is usually made of nafion. The polymer membrane consists of a porous layer of teflon with SO_3H groups as side chains. The side chains make the electrolyte selectively conductive to protons. The thickness of the membrane varies from 60 to 250 μm [3]. The membrane along with the electrodes constitutes the membrane electrode assembly (MEA) as shown in Fig. 1.1.

The electrodes (anode and cathode) are fabricated from porous carbon. Carbon is impregnated with platinum (Pt) which acts as catalyst for electrochemical reactions. The thickness of the catalyst layer (CL) is usually between 10-70 μm [2].

The bipolar plates (BP) are fabricated from graphite and stainless steel. It acts as a collector of external current. The BP contains flow channels to feed the reactant gases to the anode and cathode. It also helps to assemble different fuel cells to form a fuel cell stack.

The gas diffusion layers (GDL) is fabricated from porous carbon layer with a thickness varying from 0.2-0.5 mm [2]. It acts as a mechanical support for the CL. It also helps in the proper distribution of the reactants to the respective electrodes and the removal of product water through the flow channels.

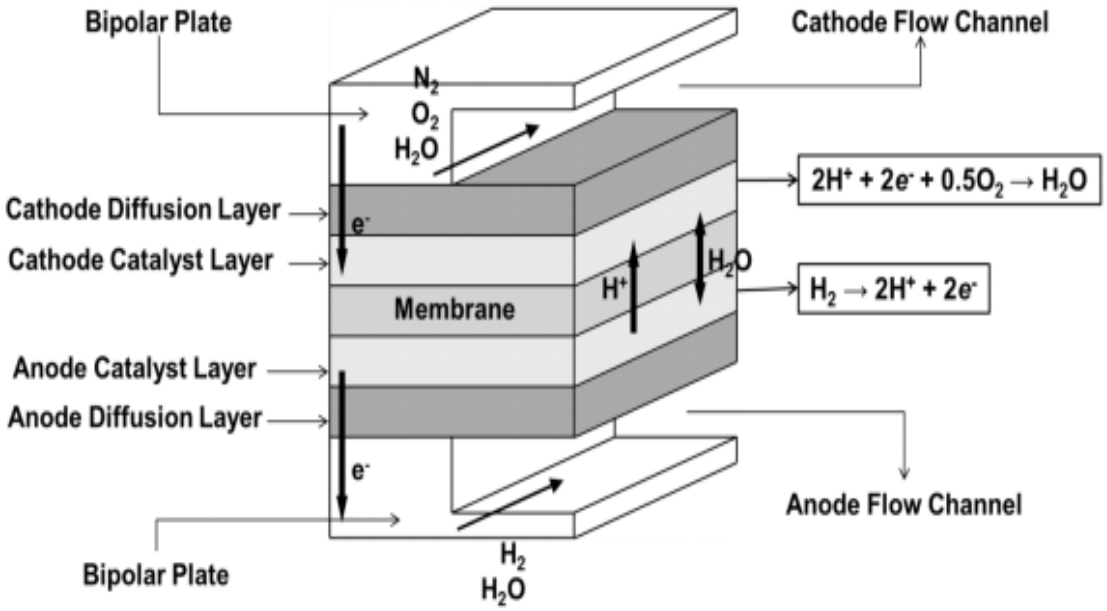

Fig. 1.1. Schematic diagram of a PEMFC [3].

1.3 Operating Principle

Humidified hydrogen is supplied to the anode gas channel. It then diffuses through the GDL on the anode side to reach the anode catalyst layer (ACL). The oxidation of hydrogen takes place in the ACL in the presence of platinum catalyst. The reaction is shown below:

$$H_2 \longrightarrow 2H^+ (aq.) + 2e^- \quad (1.1)$$

The nafion membrane selectively allows protons (H^+) ions to pass through it but it is impervious to the electrons and hydrogen gas. The electrons get collected on the anodic plate and move through the external circuit to reach the cathodic bipolar plate thus constituting an external electric current.

Humidified oxygen or humidified air is supplied to the cathodic flow plate which along with the electrons flows through the GDL to reach the cathode catalyst layer (CCL). The protons reach the CCL through the membrane. The oxygen reduction reaction occurs in the CCL over platinum catalyst:

$$\tfrac{1}{2} O_2 + 2e^- + 2H^+ (aq.) \longrightarrow H_2O (l) \quad (1.2)$$

The overall reaction can be written as:

$$H_2 + \tfrac{1}{2} O_2 \longrightarrow H_2O (l) \quad (1.3)$$

A PEMFC converts the Gibbs free energy associated with the chemical reaction into electrical energy.

Hence,

$$W_{elec} = -\Delta G \quad (1.4)$$

Where, $W_{elec}$is the maximum electrical work done by the system under conditions of constant temperature and pressure. ΔG is the Gibbs free energy associated with reaction (1.3).

$$W_{elec} = E \times Q \quad (1.5)$$

where, E is the electric potential across the fuel cell and Q is the charge carried by the external circuit.

$$Q = n \times F \tag{1.6}$$

where, n is the number of electrons which are transferred through the external circuit and F is the faraday's constant having a value of 96485 coulombs. Hence,

$$\Delta G = -n \times F \times E \tag{1.7}$$

The maximum theoretical efficiency of a PEMFC is calculated as:

$$\eta = \frac{\Delta G}{\Delta H} \tag{1.8}$$

where, ΔH is the enthalpy of the reaction (1.3). At standard pressure and a temperature of 25^0C, the efficiency is obtained to be 73 % and the open circuit potential is 1.3 V.

1.4 Anode catalyst and hydrogen oxidation reaction

The anode catalyst breaks down the gaseous hydrogen into protons and electrons. The reaction is shown as follows:

$$H_2 + Pt \rightarrow Pt + H^+ + e^- \tag{1.9}$$

The rate constant of an electrochemical reaction is directly proportional to its exchange current density. The exchange current densities of HOR and oxygen reduction reaction (ORR) are 0.1 A/cm^2 and 6μ A/cm^2 respectively [4]. Therefore, ORR is more sluggish than HOR because the exchange current density for HOR is greater than ORR.

The hydrogen that is supplied to the anode contains trace amounts of CO in it. This carbon monoxide is produced during reforming of fuels used to produce H_2. CO even when present in trace amounts (less than 1 ppm) reduces catalyst activity. Therefore, other catalysts for HOR are being developed that show greater tolerance to CO like Ruthenium, tin, tungsten and molybdenum [5].

1.5 Cathode catalyst and oxygen reduction reaction

As mentioned in the section 1.4, platinum is considerably less active for ORR than HOR. Therefore, higher platinum loading is required for the CCL than the ACL. Despite this, platinum remains the most economically viable catalyst for ORR.

The CCL consists of both micro pores and mesopores. This presence of pores on different scales makes it difficult to develop a correct theoretical model that takes into account this complex morphology. For simplification, various models for CCL have been proposed which are reviewed in section 1.7.

1.6 PEMFC performance

A PEMFC operating at 25 °C and 1 atm develops a potential difference of 1.23 V across its terminals [4]. The maximum potential difference that can be developed by an individual cell is known as reversible cell potential. But the actual voltage of the cell is always lower than the reversible cell potential because of various voltage losses. These losses are known as overpotentials. The different types of overpotentials are discussed below.

1.6.1 Activation overpotential

The activation overpotential results from the slowness of electrochemical reactions that occurs at the anode and cathode. The activation overpotential for the ACL is insignificant to the overall performance of the PEMFC. The activation overpotential of the CCL is crucial in determining the performance of PEMFC. The activation overpotential increases steeply at low current densities but remains almost constant at moderate to high current densities.

1.6.2 Ohmic overpotential

Ohmic overpotential results from the resistance of various cell components to the transfer of the electrons and protons. The ohmic overpotential increases linearly with the rise in current.

1.6.3 Concentration overpotential

Concentration overpotential results due to mass transfer limitations. It is particularly significant at high current densities.

A typical voltage-current (V-I) curve for a PEMFC along with the regions where various overpotentials are significant is presented in Fig 1.2.

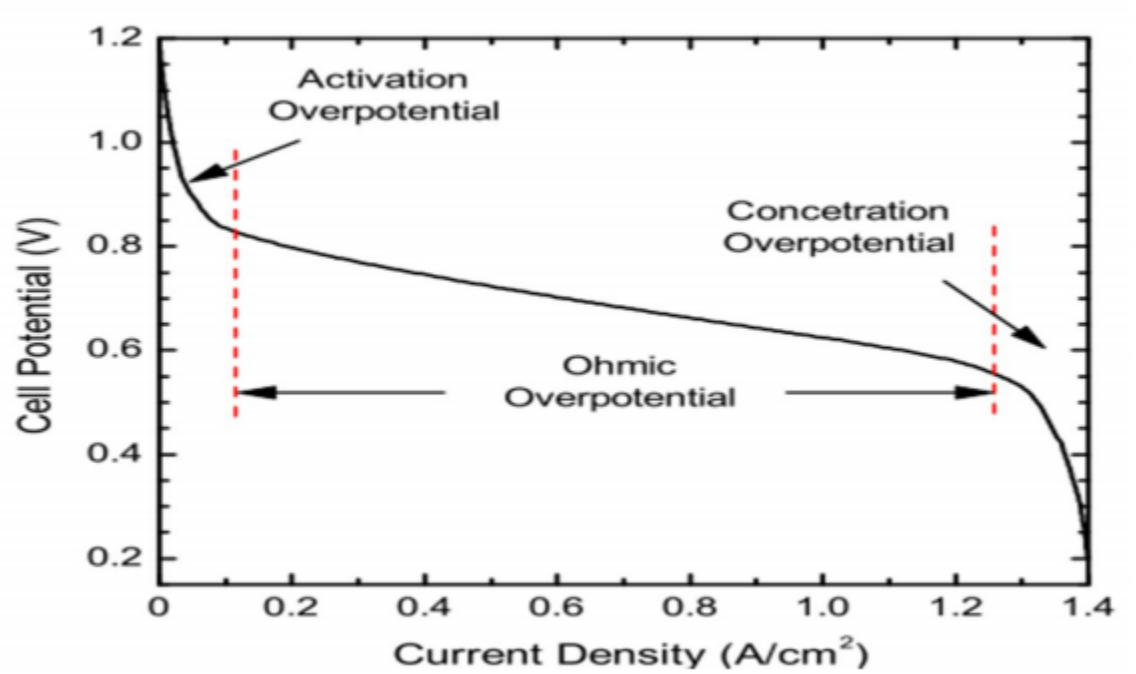

Fig. 1.2. Polarization curve for a PEMFC [6].

1.7 CCL models

Primarily three CCL models have been reported in the literature. All these models differ in their complexity based on the assumptions made to develop the model.

1.7.1 Thin film model/ Interface model

Thin film model is the simplest CCL model. This model assumes the CL as an infinitely thin layer between the polymer membrane and the GDL. It does not take into account the CL structure and assumes average values for the mass and charge transport parameters to calculate overpotential. A major advantage of interface model is that it requires less computational power during simulation. This is beneficial for developing a model for the entire PEMFC. For example, Berning and Djilali [7] developed a 3-D interface model of the PEMFC to investigate the effect of parameters like GDL porosity and CL thickness on fuel cell performance.

1.7.2 Pseudo-homogenous model/ Macro-homogenous model

The macro-homogenous model was first proposed by Tiedemann and Newman [8]. The basic assumption of this model is that the CL is a homogenous entity consisting of nafion ionomer, Pt/C catalyst and the pores. It takes into account the transport of oxygen, electrons, protons and water inside the CL and hence provides a much better estimation of the activation overpotential than the thin film model. At low current densities, the polarization losses predicted by pseudo-homogenous model are close to experimental results. But it overestimates the value of the polarization losses at high current densities.

1.7.3 Agglomerate model

The agglomerate model was first proposed by Ridge et.al [9]. This model provides the closest approximation to the actual CL morphology as seen through the SEM and TEM images. Simulations done using the agglomerate model provides better results for activation overpotential than the macro-homogenous model, particularly at higher current densities. In an agglomerate model, it is assumed that the carbon particles impregnated with platinum (Pt/C) group together to form small agglomerates. These agglomerates are usually assumed to be spherical but some researchers have used cylindrical agglomerates as well. The size of the agglomerates is found to vary between 0.02-10 μm [3]. Two types of pores are considered in an agglomerate model.

1.7.3.1 Primary Pores

The pores between the carbon particles in single agglomerate constitute the primary pores. The primary pores are usually assumed to be completely filled with nafion ionomer.

1.7.3.2 Secondary Pores

The different agglomerates are bonded by the ionomer which forms a thin film around the agglomerate. The void spaces between the different agglomerates constitute the secondary pores. These secondary pores can be partially or completely flooded with water.

1.9 Objectives

Cathode catalyst layer plays a crucial role in determining the cost and performance of a PEMFC. The performance of the CCL is influenced by various operational parameters like temperature, pressure, air composition and humidity as well as structural parameters like platinum loading, ionomer volume fraction, CL thickness, flow geometry etc. It is expensive and time consuming to perform experiments which cover the whole design space. Further, the cost of a PEMFC is mainly determined by platinum loading and ionomer fraction of the CCL. Therefore, it is important to optimize these two parameters to maximize current density.

Hence, it becomes important to develop theoretical models which take into account the morphology of the CL and the various phenomena occurring inside the PEMFC cathode.

The present study focuses on the modeling of the CCL using a comprehensive agglomerate model. This model can be reduced to a pseudo-homogenous model when the agglomerate radius approaches zero.

The objectives of the present work include:

1. To study the performance of CCL in terms of voltage-current (V-I) relationship using an agglomerate model.
2. To compare the performance of agglomerate model with the pseudo-homogenous model.
3. To study the effect of various parameters on the performance of the CCL.

CHAPTER-2
LITERATURE REVIEW

This chapter deals with the review of important research work done in the modeling of the PEMFC cathode using thin-film, pseudo-homogenous and agglomerate models. The effect of different parameters on PEMFC performance as reported in the literature is also studied. The limitations of the earlier models are also discussed in this chapter.

Wilson and Gottesfeld [10] developed a thin film model for the CCL of a PEMFC. Nafion electrolyte embedded thin film CL was considered. Simulations for variation in cell potential with current density were carried out at different values of platinum loading. The optimum platinum loading was found to be about 0.3 mg/cm^2. The main limitation of this model was that it cannot be used to find the distribution of current density or oxygen concentration inside the CL.

Rho et al. [11] reported a 1-D interface model for the PEMFC cathode. The model was solved for different combination of cathode feed composition- oxygen/nitrogen, oxygen/argon and oxygen/helium. The effect of gas pressure on PEMFC performance was also investigated. The polarization losses for the case of oxygen/helium were found to be lowest among the three cases studied. The small size of helium facilitated better transport of the gas through the CL. It was found that increase in gas pressure improved the performance of the PEMFC.

1-D steady state PEMFC model based on pseudo-homogenous model of CCL was presented by Springer et.al [12]. The results showed that the oxygen resistance was become higher with increase in current density. The optimum CL thickness was found to be 30 μm. This optimum value of CL thickness was validated from experimental results. This model was an improvement upon the thin-film model which ignored the detailed structure of the CL. However, at high current densities, the model results showed considerable variation from experimental results.

Bernardi and Vebrugge [13] developed a pseudo-homogenous model to study the effect of CL porosity on PEMFC performance. It was found that the current density almost dropped down to

zero below a porosity value of 20%. But this model did not account for the mass transfer of oxygen inside the pores because the pores were assumed to be completely saturated.

Marr and Li [14] investigated the effect of platinum loading, nafion loading and CL thickness on PEMFC performance using a pseudo-homogenous model. The optimum nafion fraction was found to be 0.55. The platinum loading and CL thickness were taken as 4 mg/cm^2 and 5 μm respectively. The optimum Pt/C ratio was found to be 0.35 and was independent of the current density. It was also observed that increase in CL thickness beyond the optimum point led to a decrease in cell voltage due to increased ohmic losses.

Eikerling and Kornyshev [15] considered a pseudo-homogenous model for the CCL. Analytical expressions were developed for four limiting conditions- small current densities, large current densities, high ionomer fraction and high porosity. The variation of current with distance was analyzed for the above four cases. The effects of oxygen pressure, nafion fraction, CL thickness and kinetic parameters on fuel cell performance were investigated. An analytical solution was developed for the active layer thickness. Active layer thickness is defined as the distance from the CL-membrane interface where the oxygen concentration drops to zero. It was observed that the oxygen diffusion significantly contributed to the polarization losses at high current densities. It was concluded that an optimum value of nafion fraction must exist which maximizes the current density. Since the analytic expressions were developed for only the limiting cases, this model could not be used to find the polarization curve for a general case.

Kulikovsky [16] has proposed a 2-D steady state pseudo-homogenous model for the CCL. An analytical expression was developed for two limiting cases: weak oxygen transport and fast oxygen transport. Tafel equation was used to describe the kinetics of oxygen reduction. The analytical solution to the governing differential equations was compared with the results obtained from numerical solution of these equations. V-I relationship was calculated for two different values of Pt/C ratio- 50% and 100%. It was found that a dead region existed near the CL-membrane interface where the reaction rate is zero. The catalyst can be removed from this region without any significant loss of voltage. This model was an improvement upon the previous one-dimensional pseudo-homogenous models. However, this model failed to provide a general solution to the governing equations.

Song et al. [17] presented a 1-D pseudo-homogenous model for the CCL. The main objective of the paper was to obtain optimum values of parameters like ionomer volume fraction, platinum loading, CL porosity and CL thickness. The optimization was done by taking two parameters simultaneously while taking the values of other parameters as constant. It was found the cathode performance is most sensitive to the CL thickness. The second most sensitive parameter was found to be platinum loading. The optimum values of ionomer volume fraction, platinum loading and CL thickness was observed 0.24 mg/cm^2, 0.087 and 13.1 μm respectively.

Secenell et al. [18] presented a pseudo-homogenous model for the CCL. The model was two-dimensional and the simulations were done using a finite element method with adaptive grid sizes. A multi-variable optimization program was used to calculate the optimum values for platinum loading, ionomer volume fraction, GDL porosity and CL thickness. The optimization was done using a gradient-based method. It was found that for a given potential, the current density increased by about 50% from the base conditions at optimum values of the above parameters. The effect of ionomer volume fraction was found to be not significant at low current densities.

In another paper, Secenell et al. [19] developed a similar model but has considered an agglomerate model for CCL rather than a pseudo-homogenous model. In addition to the parameters in the above paper, two new parameters were taken into account- agglomerate radius and ionomer film thickness. The optimization was performed for low, medium and high current densities and different values of optimal parameters were found for each case. It was observed that the optimal nafion fraction increased with current density while the optimal platinum loading was found to decrease with current density. The optimal values for platinum loading, ionomer volume fraction, CL porosity, CL thickness and GDL porosity were found to be dependent on the values of agglomerate radius and ionomer thickness. It was found that the Pt/C ratio remains almost unaffected by agglomerate radius but the optimum platinum loading first decreased and then increased with an increase in the agglomerate radius. The optimum value of nafion fraction was found to be 22.05% at medium current densities.

Dalasm et.al [20] presented a pseudo-homogenous model to investigate the effect of different catalyst parameters on cathode layer performance. The effect of seven parameters was analyzed: platinum loading, Pt/C ratio, ionomer volume fraction, CL porosity, CL thickness, porosity of

GDL, percentage penetration of GDL into the cathode layer. It was observed that the best performance was observed for a narrow range of platinum loading. Also, it was found that the CL was only utilized up to a thickness of 15 μm for current densities greater than 50 mA/cm^2. The sensitivity of platinum loading, Pt/C ratio, ionomer fraction, CL thickness, percentage penetration of GDL into the cathode layer and GDL porosity to cell voltage was found to be 0.015, 0.025, 0.35, 0.07, 0.01 and 0 respectively. The main limitation of this model is that it did not take percentage liquid saturation of the pores into account.

Ridge et.al [9] developed an agglomerate model for the CCL of a PEMFC. Diffusion of both oxygen and hydrogen ions were taken into account. The model was solved for different sets of platinum loading, ionomer fraction, electronic conductivity, GDL porosity and agglomerate radius. The results showed that GDL porosity and electronic conductivity have negligible effect on PEMFC performance. It was also observed that decrease in agglomerate radius resulted in an increase in cell voltage for the same current density. It was also observed that proton transport had a greater effect on cell performance than oxygen diffusion. However, this model did not accounted for liquid water flooding of the pores.

Iczkowski and Cutlip [22] developed an agglomerate model for PAFC cathode. The model accounted for the transport process associated with oxygen but the diffusion of protons was not taken into consideration. Whereas the previous model did not account for water flooding, flooding was taken into account in this model. It was found that gas diffusion contributes to 40% and ohmic losses contribute to 50% of the net polarization losses. The diffusion losses were found to be more prominent at high current densities. However, diffusion of protons into the agglomerate was not accounted in this model.

Broka and Ekdunge [23] compared the agglomerate model and the pseudo-homogenous model. The results were obtained for different values of oxygen diffusivity, protonic conductivity and CL thickness. Both the models were found to predict nearly the same cell voltage at low current densities. But at high current densities, the pseudo-homogenous model over predicted the electrode potential compared to the experimental results. It was concluded that the concentration overpotential was not satisfactorily accounted by the homogenous model. SEM studies were performed and images were found to bear a closer resemblance to the agglomerate model than the pseudo-homogenous model.

Seigel et al. [24] developed a 2-D model for the PEMFC based on an agglomerate model for the CL. In addition to transport and reaction kinetics of protons, electrons and oxygen, energy balance in the PEMFC and transport of water were also considered in this model. The catalyst morphology was reconstructed from a microscopic image of the membrane electrode assembly. It was found that PEMFC performance was highly dependent on ionomer volume fraction. It was observed that a decrease in agglomerate size increased current density of the fuel cell. The optimal void fraction was found out to be 0.04 and was found to be independent of the current density.

Yin [25] developed an agglomerate model for the CCL. The effect of feed gas composition, polymer electrolyte loading (ionomer volume fraction), platinum loading, CL porosity and CL thickness on current density was investigated in this study. It was observed that a low ionomer volume fraction reduced the performance of PEMFC due to poor ionic conductivity and reduction in catalytic activity. A very high electrolyte loading was also found to result in poor performance. The optimum value of the electrolyte loading was found to be 0.21.

Harvey et.al [26] compared the three CCL models by developing a 3-D model for the PEMFC. The thin film was found to over predict the current density in comparison with the other two models. The current density was observed to be over predicted by the pseudo-homogenous model as compared to the agglomerate model. The agglomerate model was found to predict significant mass transfer losses even at low current densities. It was concluded that the mass transfer limitations which were earlier observed to be significant at only high current densities are also crucial at low current densities.

Wang et al. [27] investigated the species mass transport and reaction kinetics inside spherical agglomerate. The simulations for variation in current density, oxygen concentration and activation overpotential along the radial direction were carried out for two types of spherical agglomerates. The pores were completely filled with electrolyte in the first agglomerate. This case could be seen as a limiting case of fast proton transport. An analytical expression for concentration, current and potential gradient was developed for the first type of agglomerate. The second agglomerate consisted of pores which are partially filled with water. A numerical solution was developed for this case. It was observed that the ionomer filled agglomerate has a better effectiveness than the water filled agglomerates. However, the effectiveness of water filled

agglomerates was better the ionomer filled agglomerates for a cathodic transport coefficient greater than one. It was found that the reaction rate fell by 50% within 15% of the agglomerate radius. The catalyst utilization was found to be greater for the water filled agglomerate. However, the performance of the entire cathode layer could not be predicted by the model because the model was developed for a single agglomerate.

Kamarajugadda and Mazumder [28] investigated the effect of platinum loading, ionomer fraction, Pt/C ratio, agglomerate radius and CL thickness by developing a two dimensional agglomerate model for the PEMFC cathode. It was observed the optimum value of platinum loading and ionomer fraction depended on the values of other parameters like agglomerate radius and CL thickness. Hence, it was suggested that the optimization routine should take all the parameters into account simultaneously rather than considering one or two parameters at a time. It was found that the optimum value of the parameters were different for low, medium and high current densities. The sensitivity analysis showed that the overpotential was mainly due to electrical conduction and mass transport limitations at low current densities. But these losses were mainly due to mass transport limitations at high current densities.

Another paper by Kamarajugadda and Mazumder [29] compared single radius agglomerate with overlapping spherical agglomerates of different radii. The results showed that the shape of agglomerate is insignificant to cathode performance at small agglomerate radius. However, the current density predicted by the two models differed by as much as 38% for larger agglomerates.

Sun et al. [30] presented a 2-D PEMFC model based on an agglomerate model for the CCL. The effect of nafion fraction, platinum loading, agglomerate radius and ionomer film thickness on the electrode potential was investigated. It was found the cell potential decreased with increase in ionomer film thickness and agglomerate radius. The optimum value of nafion fraction was found to be 0.23.

Epting and Litster [31] developed an agglomerate model for the PEMFC cathode. But instead of a single agglomerate radius, the CL was assumed to contain agglomerates of different radii which obey a Gaussian style size distribution curve. The results showed the current density predicated by single radius agglomerate model and multiple radius agglomerate model with the

same mean radius could differ by as much as 65%. However, at low agglomerate radius, this difference was found to be insignificant.

Das et.al [32] investigated the influence of spatial distribution of the spherical agglomerates on the polarization losses in PEMFC cathode. Three different arrangements were considered: in-line, staggered along x-axis and staggered along both x and y axes. A considerable difference in current densities was found in the three cases studied. The staggered arrangement was found to result in greater activation losses than an in-line arrangement.

Dalasm et.al [33] developed a rigorous model for the CCL of a PEMFC. The effect of three operational parameters- operating temperature, oxygen pressure and percentage flooding of the pores as well as eight structural parameters- platinum loading, Pt/C ratio, ionomer fraction, agglomerate radius, ionomer film thickness, CL thickness, GDL porosity and GDL penetration in the pores. The relative effect of each parameter was studied. An optimization routine was developed to calculate the optimum value of these parameters. It was observed by sensitivity analysis that the PEMFC performance was most affected by the CL thickness. The optimum values of liquid saturation, platinum loading, Pt/C ratio, ionomer fraction, agglomerate radius, ionomer film thickness, GDL porosity, GDL penetration and CL thickness were found to be 0, 0.06 mg/cm^2, 0.33, 0.074, 0.374 μm, 0 nm, 0.45, 0.05 and 70 μm respectively.

CHAPTER-3
MODEL DEVELOPMENT

A 1-D steady-state model for the CCL of a PEMFC is developed by considering an agglomerate model. The overall transport phenomena and the electrochemical kinetics of each species namely oxygen, electrons and protons inside the CCL is studied. The effect of two operational parameters and five structural parameters on the performance of the cathode is investigated. The parameters are as follows:

Operational Parameters:

1. Operating temperature.
2. Operating pressure.

Structural Parameters:

1. Agglomerate radius
2. Ionomer film thickness.
3. Platinum loading.
4. Ionomer volume fraction (nafion loading).
5. CL thickness.

To develop this model, the following assumptions have been made:

1. The CL consists of homogenous agglomerates having identical properties.
2. The agglomerate is assumed to be spherical.
3. The agglomerate is surrounded by an ionomer film of fixed thickness.
4. The primary pores are completely filled with the nafion ionomer.
5. The secondary pores are completely saturated with water (fully flooded condition).
6. The electrochemical reactions occur under isothermal conditions.
7. The operation is in steady state.
8. The GDL is assumed to be thin and any mass transfer effects through it are neglected.
9. The feed to the cathode is pure oxygen.

A schematic diagram of the present model is shown in Fig. 3.1. It can be observed from the figure that the spherical agglomerate is surrounded by an ionomer film of uniform thickness. The carbon particles are distributed inside the agglomerate in an irregular fashion.

The oxygen which is supplied to cathode gas channels diffuses through the GDL to reach the CL-GDL interface. Since the pores are completely flooded, oxygen dissolves in liquid water and diffuses through the pores to reach the surface of ionomer film. The oxygen then dissolves in the ionomer film and penetrates it to reach the agglomerate surface. It then diffuses through the agglomerate to reach the reaction sites.

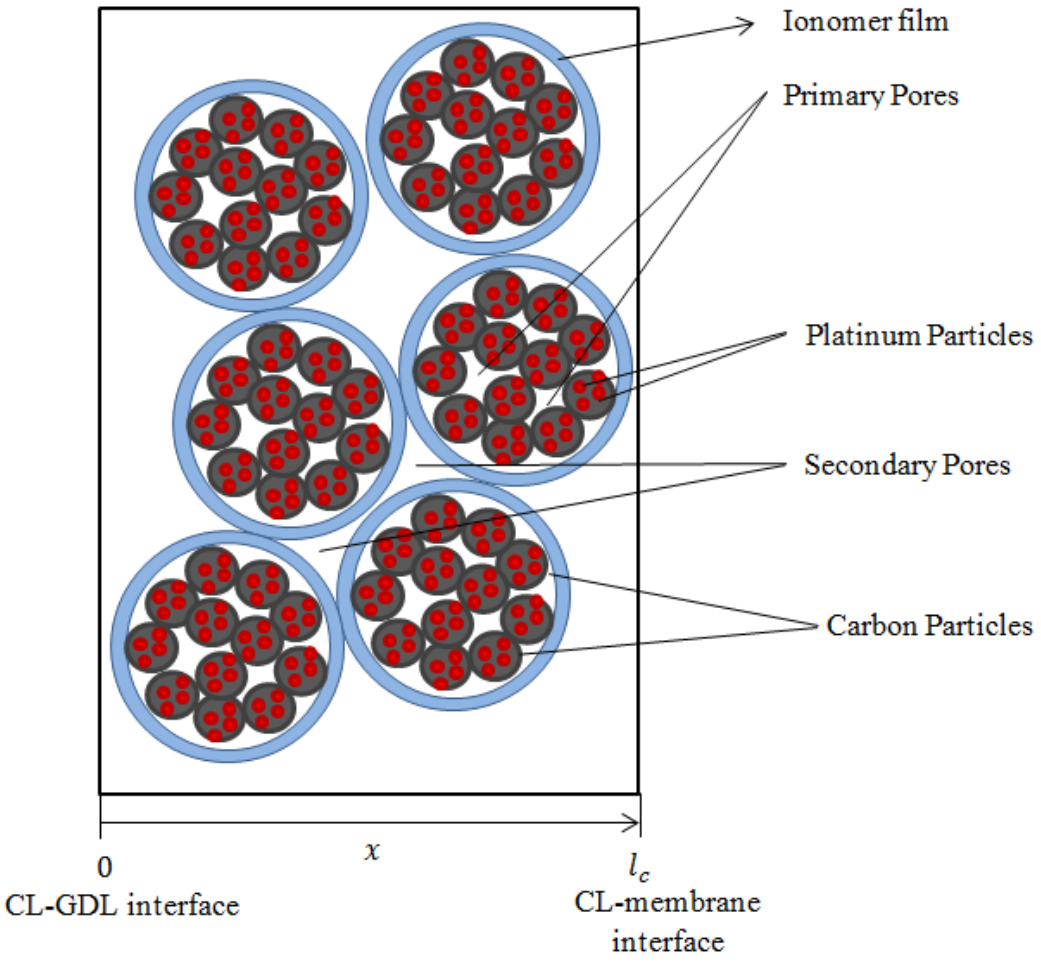

Fig. 3.1. Schematic of the present model.

In this mathematical model, equations are developed which account for the reaction kinetics and transport of oxygen, electrons and protons. The reaction kinetics is given by Butler-Volmer equation. The mass transfer of oxygen is governed by Fick's law. The transport of electrons and protons in the CCL is governed by Ohm's law.

The model development is divided into three sections that forms the basis of three ordinary differential equations in terms of current density, dissolved oxygen concentration and activation overpotential.

3.1 Electrochemical reaction rate (Butler-Volmer equation)

The final equations which describe the electrochemical reaction rate are derived in sections 3.2.1 to 3.2.4

3.1.1 Oxygen diffusion inside the agglomerate

On applying mole balance on oxygen inside spherical agglomerate under steady- state conditions, the following equation is obtained:

$$\nabla . N_{O_2} = R_{O_2} \tag{3.1}$$

Where R_{O_2} is the oxygen consumption rate inside the agglomerate and N_{O_2} is the molar flux of oxygen in the radial direction. Applying Fick's law, we get:

$$N_{O_2} = -D_{O_2,m}^{eff} \nabla C_{O_2} \tag{3.2}$$

In equation (3.2), $D_{O_2,m}^{eff}$ is the effective oxygen diffusion coefficient within the agglomerate. It is described by Bruggeman correlation [34]:

$$D_{O_2,m}^{eff} = {\varepsilon_{agg}}^{1.5} D_{O_2,m} \tag{3.3}$$

where, ε_{agg} is the volume fraction of the ionomer inside the agglomerate and $D_{O_2,m}$ is the bulk diffusivity of oxygen dissolved in the electrolyte. $D_{O_2,m}$ is given by the following empirical correlation [14]:

$$D_{O_2,m} = -1.0664 * 10^{-5} + 9.0215 * 10^{-6} * \exp\left(\frac{T-273}{106.65}\right)\frac{cm^2}{s} \quad (3.4)$$

The rate of reaction R_{O_2} is first order with respect to oxygen concentration. Hence, it can be expressed as:

$$R_{O_2} = -kC_{O_2} \quad (3.5)$$

where, k is the reaction rate constant. The negative sign represents that the oxygen is being consumed in this electrochemical reaction.

Combining equations (3.1), (3.2) and (3.5), result in equation (3.6) as shown below:

$$\nabla.\left(\mathrm{D}_{\mathrm{O_2,m}}^{\mathrm{eff}}\nabla\mathrm{C}_{\mathrm{O_2}}\right) - \mathrm{kC}_{\mathrm{O_2}} = 0 \quad (3.6)$$

Assuming only radial gradients of oxygen concentration, equation (3.6) can be expressed as:

$$\frac{D_{O_2,m}^{eff}}{r^2}\left(\frac{d}{dr}r^2\left(\frac{dC_{O_2}}{dr}\right)\right) - kC_{O_2} = 0 \quad (3.7)$$

Equation (3.7) represents a second order ODE with the following boundary conditions:

$$\frac{dC_{O_2}}{dr} = 0 \; at \; r = 0$$
$$C_{O_2} = C_{O_2,ag-film} \; at \; r = r_{agg} \quad (3.8)$$

where, $C_{O_2,ag-film}$ is the concentration of oxygen at the agglomerate-ionomer film interface and r_{agg} is the radius of single agglomerate.

To obtain an analytical solution for equation (3.7), it is first changed into a dimensionless form.

$$\frac{1}{r^2}\left(\frac{d}{dr}r^2\left(\frac{dC_{O_2}}{dr}\right)\right) - \frac{k}{D_{O_2,m}^{eff}}C_{O_2} = 0 \quad (3.9)$$

In place of radius r and dissolved oxygen concentrationC_{O_2}, new dimensionless variables are defined as follows:

$$\bar{r} = \frac{r}{r_{agg}} \quad (3.10)$$

$$\overline{C_{O_2}} = \frac{C_{O_2}}{C_{O_2,ag-film}} \tag{3.11}$$

Combining, equations (3.9), (3.10) and (3.11)

$$\frac{1}{\bar{r}^2}\left(\frac{d}{d\bar{r}}\bar{r}^2\left(\frac{d\overline{C_{O_2}}}{d\bar{r}}\right)\right) - \frac{{kr_{agg}}^2}{D_{O_2,m}^{eff}}\overline{C_{O_2}} = 0 \tag{3.12}$$

A dimensionless group φ is defined as:

$$\varphi = r_{agg}\sqrt{\frac{k}{D_{O_2,m}^{eff}}} \tag{3.13}$$

The modified boundary conditions are:

$$\begin{aligned} &\frac{d\overline{C_{O_2}}}{dr} = 0 \; at \; \bar{r} = 0 \\ &\overline{C_{O_2}} = 1 \; at \; \bar{r} = 1 \end{aligned} \tag{3.14}$$

By combining equations (3.12) and (3.13), the following equation is obtained:

$$\frac{1}{\bar{r}^2}\left(\frac{d}{d\bar{r}}\bar{r}^2\left(\frac{d\overline{C_{O_2}}}{d\bar{r}}\right)\right) - \varphi^2\overline{C_{O_2}} = 0 \tag{3.15}$$

Equation (3.15) can be expanded as:

$$2\bar{r}\frac{d\overline{C_{O_2}}}{d\bar{r}} + \bar{r}^2\frac{d^2\overline{C_{O_2}}}{d\bar{r}^2} - \varphi^2\overline{C_{O_2}}\bar{r}^2 = 0 \tag{3.16}$$

Rearranging the above equation, we get:

$$2\frac{d\overline{C_{O_2}}}{d\bar{r}} + \bar{r}\frac{d^2\overline{C_{O_2}}}{d\bar{r}^2} - \varphi^2\overline{C_{O_2}}\bar{r} = 0 \tag{3.17}$$

By defining a new variable, $\bar{u}$ as:

$$\bar{u} = \overline{C_{O_2}}\bar{r} \tag{3.18}$$

$$\frac{d\bar{u}}{d\bar{r}} = \bar{r}\frac{d\overline{C_{O_2}}}{d\bar{r}} + \overline{C_{O_2}} \tag{3.19}$$

Hence,

$$\frac{d^2\bar{u}}{d\bar{r}^2} = 2\frac{d\overline{C_{O_2}}}{d\bar{r}} + \bar{r}\frac{d^2\overline{C_{O_2}}}{d\bar{r}^2} \tag{3.20}$$

Combining equations (3.17), (3.18) and (3.20) results in the following second order ordinary differential equation:

$$\frac{d^2\bar{u}}{d\bar{r}^2} - \varphi^2\bar{u} = 0 \tag{3.21}$$

This is a standard ODE whose solution is given by:

$$\bar{u} = C_1 \cosh\varphi\bar{r} + C_2 \sinh\varphi\bar{r} \tag{3.22}$$

So,

$$\overline{C_{O_2}} = \frac{\bar{u}}{\bar{r}} \tag{3.23}$$

On applying the relevant boundary conditions to equation (3.23) as given by equation (3.14) , the values of C_1 and C_2 can be obtained by solving two simultaneous linear equations.

$$C_1 = 0 \tag{3.24}$$

$$C_2 = \frac{1}{\sinh\varphi} \tag{3.25}$$

Hence,

$$\overline{C_{O_2}} = \frac{\sinh\varphi\bar{r}}{\bar{r}\sinh\varphi} \tag{3.26}$$

3.1.2 Mean reaction rate

The mean reaction rate is defined as:

$$\text{Mean reaction rate}\left(\frac{\frac{\text{mol}}{\text{m3}}}{\text{s}}\right) = \frac{\text{Total oxygen consumption inside the agglomerate}}{\text{Volume of the agglomerate}}$$

Mathematically, the above statement can be written as:

$$R_{O_2,mean} = \frac{\int_0^{r_{agg}} 4\pi r^2 R_{O_2}}{V_{agg}} \tag{3.27}$$

where, $R_{O_2,mean}$ is the mean volumetric consumption rate of oxygen and V_{agg} is the volume of single agglomerate particle.

$$V_{agg} = \frac{4}{3}\pi r_{agg}^3 \tag{3.28}$$

By integration, $R_{O_2,mean}$ is obtained as:

$$R_{O_2,mean} = kC_{O_2,ag-film} \times \frac{3}{\varphi}\left(\frac{1}{\tanh\varphi} - \frac{1}{\varphi}\right) \tag{3.29}$$

Defining agglomerate effectiveness factor as:

$$E = \frac{R_{O_2,mean}}{R_{O_2,max}} \tag{3.30}$$

where, $R_{O_2,max}$ is the maximum reaction rate which can be written as:

$$R_{O_2,max} = kC_{O_2,ag-film} \tag{3.31}$$

Hence, the effectiveness factor is given by:

$$E = \frac{3}{\varphi}\left(\frac{1}{\tanh\varphi} - \frac{1}{\varphi}\right) \tag{3.32}$$

3.1.3 Mass transfer of oxygen in the ionomer film

Oxygen in the secondary pores diffuses through the ionomer film surrounding the agglomerate to reach the surface of the agglomerate. The equation for mole balance of oxygen in the ionomer film can be written as:

$$\nabla . N_{O_2} = R_{O_2} = 0 \tag{3.33}$$

The reaction term for oxygen is taken as zero because no reaction takes place in the ionomer film. By applying Fick's law, the molar flux, N_{O_2} can be written as:

$$N_{O_2} = -D_{O_2,m}\nabla C_{O_2} \tag{3.34}$$

Hence,

$$D_{O_2,m}\frac{d}{dr}\left(r^2\frac{dC_{O_2}}{dr}\right)=0 \tag{3.35}$$

The boundary conditions (BCs) for the above ODE are:

$$\begin{aligned} C_{O_2} &= C_{O_2,ag-film}\ at\ r = r_{agg} \\ C_{O_2} &= C_{O_2,film-pore}\ at\ r = (r_{agg}+\delta_{agg}) \end{aligned} \tag{3.36}$$

where, δ_{agg} is the ionomer film thickness and $C_{O_2,film-pore}$ is the oxygen concentration at the boundary between the secondary pores and the ionomer film.

The general solution to ODE in equation (3.35) is given by:

$$C_{O_2}=\frac{C_3}{r}+C_4 \tag{3.37}$$

By applying the BC's given in equation (3.36), the following solution is obtained:

$$C_{O_2}=\frac{\left(C_{O_2,film-pore}-C_{O_2,ag-film}\right)\times r_{agg}\times(r_{agg}+\delta_{agg})}{\delta_{agg}}\left(\frac{1}{r}-\frac{1}{r_{agg}}\right)+C_{O_2,ag-film} \tag{3.38}$$

The molar flux at the film-pore interface is given by:

$$N_{O_2}=-D_{O_2,m}\frac{dC_{O_2}}{dr}=D_{O_2,m}\frac{r_{agg}}{(r_{agg}+\delta_{agg})}\times\frac{\left(C_{O_2,film-pore}-C_{O_2,ag-film}\right)}{\delta_{agg}} \tag{3.39}$$

The oxygen that enters the ionomer film is completely consumed inside the agglomerate. This can be mathematically written as:

$$N_{O_2}\times a_{agg}=R_{O_2,mean} \tag{3.40}$$

where, a_{agg} is the effective external area of agglomerate per unit volume of the CL.

The interface concentration $C_{O_2,film-pore}$ is linked to the concentration in the secondary pores by using Henry's law:

$$C_{O_2,film-pore}=\frac{C_{O_2,l}}{K_{O_2}} \tag{3.41}$$

Where, $C_{O_2,l}$ is the concentration of oxygen in the secondary pores and K_{O_2} is the henry's constant which is given by [13]:

$$K_{O_2} = \frac{0.1}{RT}\exp\left(\frac{-666}{T} + 14.1\right) \tag{3.42}$$

Combining equations (3.31), (3.32), (3.39), (3.40), (3.41) and (3.42), $C_{O_2,ag-film}$ can be written in terms of $C_{O_2,l}$ as:

$$C_{O_2,ag-film} = \left(1 + \frac{Ek\delta_{agg}}{a_{agg}D_{O_2,m}}\frac{r_{agg}+\delta_{agg}}{r_{agg}}\right)^{-1}\frac{C_{O_2,l}}{K_{O_2}} \tag{3.43}$$

3.1.4 Butler-Volmer equation

The kinetics of oxygen reduction is given by the Butler-Volmer equation [40]. The Butler-Volmer equation gives the first order reaction rate constant as a function of overpotential, active surface area and exchange current density.

$$k = \frac{1}{4F}\frac{A_{eff}i_{0,ref}}{C_{O_2,ref}(1-\varepsilon_c)}\left[\exp\left(\frac{\alpha_c F}{RT}\eta\right) - \exp\left(-\frac{\alpha_a F}{RT}\eta\right)\right] \tag{3.44}$$

where, A_{eff} is the active surface area per unit volume of the catalyst. $i_{0,ref}$ is the reference exchange current density which is given by [35]:

$$log_{10}i_{0,ref} = 0.03741T - 16.96\frac{A}{m^2} \tag{3.45}$$

ε_c is the CL porosity.

α_a and α_c are the anode and cathode transfer coefficients respectively.

η is the cathode activation overpotential.

3.1.5 Species mole balance

By applying mole balance for any species '*j*' over a thin strip of *dx* thickness along the length of the CL, the following equation is obtained:

$$\frac{\partial C_j}{\partial t} = -\frac{\partial N_j}{\partial x} + R_j \tag{3.46}$$

where, C_j is the concentration of *j*, N_j is the molar flux of *j* and R_j is the reaction rate. Since, the fuel cell is operated under steady state,

$$\frac{dN_j}{dx} = R_j \tag{3.47}$$

The rate of reaction of different species is in same proportion as their stoichiometric coefficients in the reaction. Hence,

$$R_{O_2} = \frac{1}{4} R_{H+} = \frac{1}{4} R_e \tag{3.48}$$

where, R_{H+} and R_e are the consumption rated of protons and electrons respectively.

Combining equations (3.47) and (3.48) results in the following equation:

$$\frac{dN_{O_2}}{dx} = \frac{1}{4}\frac{dN_{H+}}{dx} = \frac{1}{4}\frac{dN_e}{dx} \tag{3.49}$$

Since, the current density *i* is the charge equivalent of the molar flux of protons,

$$i = -N_{H+} \times F \tag{3.50}$$

The negative sign represents that the direction of current is opposite to the assumed direction of flux of protons.

From equations (3.47), (3.48) and (3.50),

$$\frac{di}{dx} = -4F R_{O_2} \tag{3.51}$$

$R_{O_2,mean}$ is defined on per unit volume of agglomerate, Hence, a correction factor $(1 - \varepsilon_c)$ has to be introduced.

$$\frac{di}{dx} = -4F(1 - \varepsilon_c)\, R_{O_2,mean} \tag{3.52}$$

By combining equations (3.29), (3.32), (3.43) and (3.52), equation (3.53) is obtained:

$$\frac{di}{dx} = 4F\left(\frac{1}{Ek(1-\varepsilon_c)} + \frac{\delta_{agg}}{a_{agg} D_{O_2,m}} \frac{r_{agg} + \delta_{agg}}{r_{agg}}\right)^{-1} \frac{C_{O_2,l}}{K_{O_2}} \tag{3.53}$$

3.2 Oxygen mass transport

From equation (3.49) and (3.50), it is observed that:

$$\frac{dN_{O_2}}{dx} = -\frac{1}{4F}\frac{di}{dx} \tag{3.54}$$

Hence,

$$\int_x^{l_c} \frac{dN_{O_2}}{dx} = \int_x^{l_c} \frac{1}{4F}\frac{di}{dx} \tag{3.55}$$

where, l_c is the location of CL-membrane interface.

Since, oxygen flux is zero at this interface, and current *i* is equal to the cell current density *I*.

$$N_{O_2} = -\frac{1}{4F}(i - I) \tag{3.56}$$

Applying Fick's Law,

$$N_{O_2} = D_{O_2}^{eff}\frac{dC_{O_2,l}}{dx} \tag{3.57}$$

From equations (3.56) and (3.57),

$$\frac{dC_{O_2,l}}{dx} = \frac{i - I}{4FD_{O_2}^{eff}} \tag{3.58}$$

As stated in the assumption 5, there are two parallel pathways for diffusion of oxygen into the CL to reach the reaction sites:

(1) Dissolution of oxygen into the secondary pores which are completely flooded with water.
(2) Dissolution of oxygen in the nafion phase.

Therefore, the effective diffusivity $D_{O_2}^{eff}$ can be mathematically expressed as:

$$D_{O_2}^{eff} = \alpha_1 D_{O_2,w}^{eff} + \alpha_2 D_{O_2,m}^{eff} \tag{3.59}$$

where, $D_{O_2,w}^{eff}$ and $D_{O_2,m}^{eff}$ are the effective oxygen diffusion coefficient through the flooded pores and ionomer phase respectively.

α_1 and α_2 are the volume fractions of the respective phases.

$$\alpha_1 = \frac{\varepsilon_c}{\varepsilon_c + L_{m,c} + L_S} \tag{3.60}$$

$$\alpha_2 = \frac{L_{m,c}}{\varepsilon_c + L_{m,c} + L_S} \tag{3.61}$$

where, $L_{m,c}$ and L_S are the volume fractions of nafion phase and solid phase respectively.

Applying Bruggeman correction,

$$D_{O_2,w}^{eff} = {\varepsilon_c}^{1.5} D_{O_2,w} \tag{3.62}$$

$$D_{O_2,m}^{eff} = {\varepsilon_c}^{1.5} D_{O_2,m} \tag{3.63}$$

$D_{O_2,m}$ and $D_{O_2,w}$ are the bulk diffusivities of oxygen in ionomer and liquid water.

$D_{O_2,w}$ is given by the Wilke-Chang equation[36] as follows:

$$D_{O_2,w} = \frac{7.4 * 10^{-11} * T(\phi M_{O_2})^{0.5}}{\mu_{H_2O} * (V_{O_2})^{0.6}} \frac{cm^2}{s} \tag{3.64}$$

where, M_{O_2} is the molecular weight of water.

V_{O_2} is the molar volume of oxygen at normal boiling point and is equal to 25.6 cm^3/mol.

ϕ is the association parameter for water-oxygen and is equal to 2.26.

T is the temperature in K.

μ_{H_2O} is the viscosity of water in Pa-s and is given by [37]:

$$\mu_{H_2O} = A \times 10^{\frac{B}{T-C}} \frac{Pa}{s} \tag{3.65}$$

where, $A = 2.414 \times 10^{-5}\ Pa - s$

$B = 247.8\ K$

$C = 140\ K$

3.3 Activation overpotential

The protons and electrons flow through the ionomer and solid phase respectively. The resistance to the flow of protons and electrons result in polarization losses. The activation overpotential is related to the protonic and electronic current densities by the Ohm's law:

$$\frac{d\eta}{dx} = \frac{i}{\kappa_{eff}} + \frac{i_e}{\sigma_{eff}} \tag{3.66}$$

where, i and i_e are the protonic and electronic current densities respectively.

κ_{eff} is the effective protonic conductivity of ionomer phase inside the CL. σ_{eff} is the effective electronic conductivity of the solid phase inside the CL.

These conductivities are related to their bulk values κ and σ by Bruggeman correlation:

$$\kappa_{eff} = {L_{m,c}}^{\tau}\kappa \tag{3.67}$$

$$\sigma_{eff} = {L_S}^{\tau}\sigma \tag{3.68}$$

From equation (3.49),

$$\frac{dN_{H+}}{dx} = \frac{dN_e}{dx} \tag{3.69}$$

By integrating the above equation from x to l_c,

$$\int_x^{l_c} \frac{dN_{H+}}{dx} = \int_x^{l_c} \frac{dN_e}{dx} \tag{3.70}$$

Using equation (3.50),

$$\int_x^{l_c} \frac{di}{dx} = \int_x^{l_c} \frac{di_e}{dx} \tag{3.71}$$

Since, the membrane does not allow the conduction of electrons, i_e vanishes at the CL-membrane interface

$$i_e = i - I \tag{3.72}$$

By combining equations (3.66) and (3.72), the following equation is obtained:

$$\frac{d\eta}{dx} = \frac{i}{\kappa_{eff}} + \frac{i - I}{\sigma_{eff}} \tag{3.73}$$

3.4 Boundary conditions

The equations (3.53), (3.58) and (3.73) constitute a system of ODE's in terms of current, oxygen concentration and activation overpotential. The boundary conditions for this system of ODEs are presented below:

$$i = 0 \; at \; x = 0 \tag{3.74}$$

This is because the protons could not travel through the external circuit. Therefore, it vanishes at the CL-GDL interface.

$$i = I \; at \; x = l_c \tag{3.75}$$

$$C_{O_2} = \frac{P_{O_2}}{H_{O_2,w}} \; at \; x = 0 \tag{3.76}$$

where, P_{O_2} is the pressure of feed oxygen and $H_{O_2,w}$ is the Henry's constant for oxygen in water.

Since the pores are assumed to be completely saturated with water, the oxygen has to first dissolve in water before reaching the reaction sites. Hence, the concentration of oxygen at the CL-GDL interface can be calculated by Henry's law as [38]:

$$H_{O_2,w} = 1.33 \exp\left(\frac{-666}{T}\right) \tag{3.77}$$

3.5 Calculation of CL porosity

$$V_t = V_m + V_C + V_{Pt} + V_P \tag{3.78}$$

where, V_t is the total CL volume. $V_m, V_C, V_{Pt}, V_P and \; V_G$ are the volumes of ionomer phase, carbon phase, platinum phase, pores and respectively.

$$\varepsilon_c = \frac{V_P}{V_t} \tag{3.79}$$

$$L_{mc} = \frac{V_m}{V_t} \tag{3.80}$$

$$L_{Pt} = \frac{V_{Pt}}{V_t} \tag{3.81}$$

$$L_C = \frac{V_C}{V_t} \tag{3.82}$$

$L_{Pt}\ and\ L_C$ are the volume fractions of carbon phase and platinum phase respectively.

$$L_S = L_C + L_{Pt} \tag{3.83}$$

$$V_{Pt} = \frac{(mass)_{Pt}}{\rho_{Pt}} \tag{3.84}$$

$$V_C = \frac{(mass)_C}{\rho_C} \tag{3.85}$$

where, $\rho_C\ and\ \rho_{Pt}$ are the densities of carbon and platinum respectively.

$$m_{Pt} = \frac{(mass)_{Pt}}{A_C} \tag{3.86}$$

$$m_C = \frac{(mass)_C}{A_C} \tag{3.87}$$

where $m_{Pt}\ and\ m_C$ are platinum mass loading and carbon mass loading respectively.

$$V_t = A_C l_C \tag{3.88}$$

$$L_{Pt} = \frac{m_{Pt}}{\rho_{Pt} l_c} \tag{3.89}$$

$$L_C = \frac{m_C}{\rho_C l_c} \tag{3.90}$$

The Pt/C ratio, f is defined as:

$$f = \frac{m_{Pt}}{m_{Pt} + m_C} \tag{3.91}$$

Hence, combining equations (3.79), (3.80), (3.89), (3.90) and (3.91), the CL porosity can be calculated as:

$$\varepsilon_c = 1 - L_{mc} - \frac{m_{Pt}}{l_c}\left(\frac{1}{\rho_{Pt}} + \frac{1-f}{f}\frac{1}{\rho_C}\right) \tag{3.92}$$

3.6 Calculation of total external area of agglomerates per unit volume of CL

By volume balance, it can be written that:

$$V_{agg,tot} = V_C + V_{Pt} + V_{m|nucleus} \tag{3.93}$$

where, $V_{agg,tot}$ is the total volume of agglomerates and $V_{m|nucleus}$ is ionomer volume inside the agglomerate.

Hence,

$$\varepsilon_{agg} = \frac{V_{m|nucleus}}{V_{agg,tot}} \tag{3.94}$$

$$V_{agg,tot} = n'_{agg}\frac{4}{3}\pi {r_{agg}}^3 \tag{3.95}$$

where, n'_{agg} is the total number of agglomerates inside the CL.

$$V_m = V_{m|nucleus} + n'_{agg}\frac{4}{3}\pi\left[\left(r_{agg} + \delta_{agg}\right)^3 - {r_{agg}}^3\right] \tag{3.96}$$

$$n_{agg} = \frac{n'_{agg}}{V_t} \tag{3.97}$$

where, n_{agg} is the number of agglomerates per unit volume of the CL.

Combining equations (3.93), (3.94), (3.95), (3.96) and (3.97)

$$n_{agg} = \frac{(1-\varepsilon_c)}{\frac{4}{3}\pi\left(r_{agg} + \delta_{agg}\right)^3} \tag{3.98}$$

and,

$$\varepsilon_{agg} = \frac{L_{mc} - n_{agg}\frac{4}{3}\pi\left[\left(r_{agg} + \delta_{agg}\right)^3 - {r_{agg}}^3\right]}{n_{agg}\frac{4}{3}\pi {r_{agg}}^3} \tag{3.99}$$

Hence, total external area of the agglomerates per unit volume of CL is given by:

$$a_{agg} = 4\pi {r_{agg}}^2 n_{agg} \tag{3.100}$$

3.7 Calculation of active surface area per unit volume of CL

A_s is the active surface area per unit mass of platinum which is related to f [20]:

$$A_s = (227.79f^3 - 158.57f^2 - 201.53f + 159.5) \times 10^3 \, m^2 \tag{3.101}$$

$$A = \frac{m_{Pt}}{l_c} A_s \varepsilon_l \tag{3.102}$$

where, ε_l is the effective platinum surface ratio and is usually taken as 0.75.

3.8 Calculation of cell voltage

The cell voltage V_{cell} is given by:

$$V_{cell} = E_{rev} - \eta - I \times R_{ohm} \tag{3.103}$$

where, R_{ohm} is the ohmic resistance of the cell. E_{rev} is the reversible cell potential given by [45]:

$$E_{rev} = 1.229 - 0.85 \times 10^3 (T - 298.15) + 4.31 \times 10^{-5} T \left(\ln\left(P_{H_2}\right) + 0.5 \ln\left(P_{O_2}\right) \right) \tag{3.104}$$

where, P_{O_2} and P_{H_2} are the partial pressures of oxygen and hydrogen respectively.

3.9 Pseudo-homogenous model

The agglomerate model reduces to a pseudo-homogenous model when the radius of agglomerate approaches zero.

Therefore,

$$\varphi = r_{agg} \sqrt{\frac{k}{D_{O_2,m}^{eff}}} = 0 \tag{3.105}$$

$$E = \frac{3}{\varphi} \left(\frac{1}{\tanh \varphi} - \frac{1}{\varphi} \right) = 1 \tag{3.106}$$

$$\frac{di}{dx} = 4F\left(\frac{1}{Ek(1-\varepsilon_c)} + \frac{\delta_{agg}}{a_{agg}D_{O_2,m}}\frac{r_{agg}+\delta_{agg}}{r_{agg}}\right)^{-1}\frac{C_{O_2,l}}{K_{O_2}} = 4Fk\frac{C_{O_2,l}}{K_{O_2}}(1-\varepsilon_c) \quad (3.107)$$

3.10 Solution methodology

The three ODE's defined in equations (3.53), (3.58) and (3.73) with the boundary conditions that are described in section 3.5 constitute a boundary value problem (BVP). This BVP is solved by using a fourth order Runge-Kutta method. A solution strategy known as shooting algorithm is used to convert the BVP into an initial value problem (IVP).

The program for the solution of these ODE's is written in Matlab2012a. Stiff solver ode15s is used to find the solution of the differential equations. The shooting algorithm is described in the Fig. 3.2.

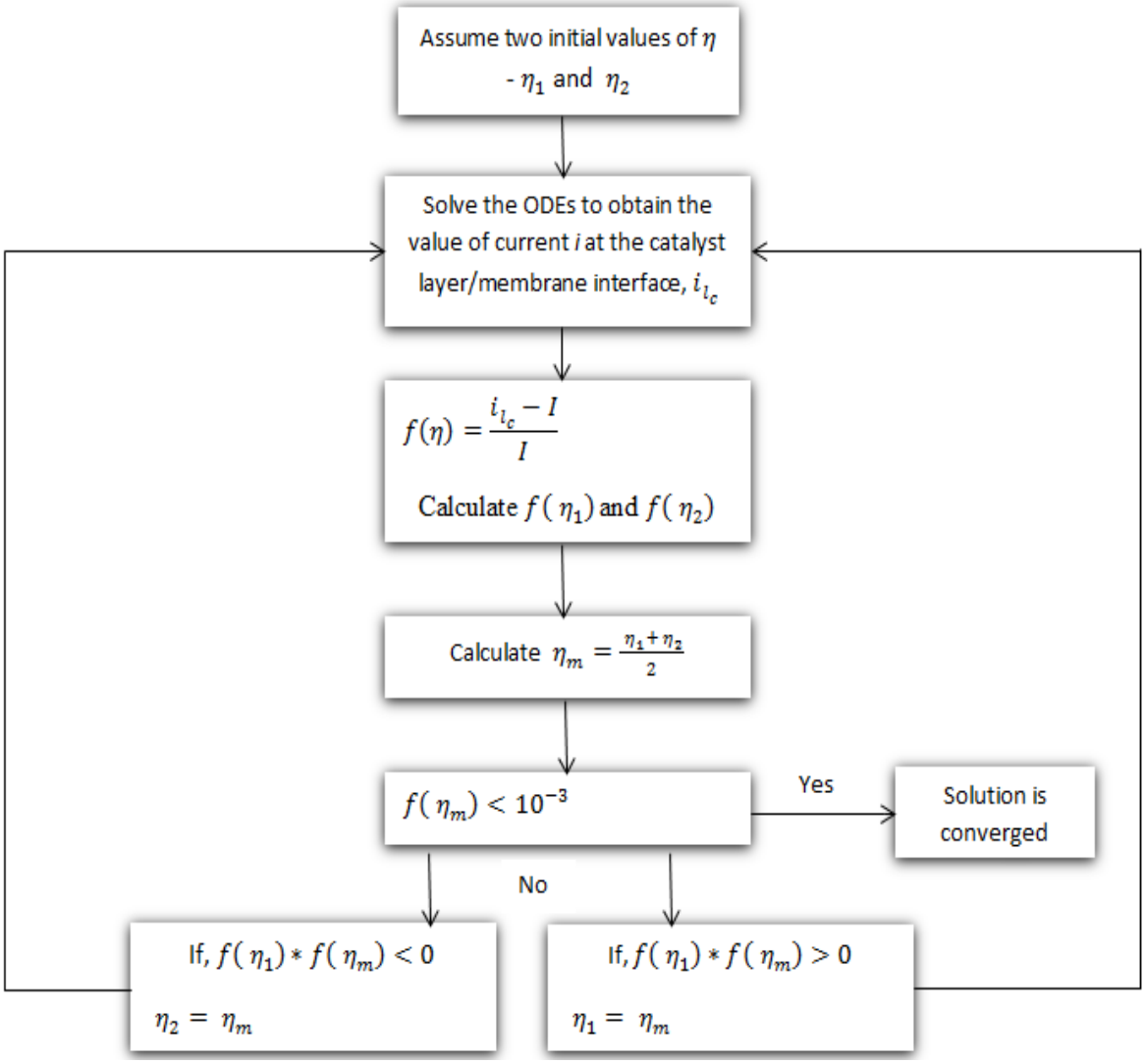

Fig. 3.2. Flowchart of the solution methodology.

CHAPTER-4
RESULTS AND DISCUSSIONS

The model described in chapter 3 consists of three first order ODEs in terms of current density, oxygen concentration and activation overpotential respectively. These equations were solved using Matlab2012a. The results obtained by solving the model equations were validated against the experimental results reported by Ticianelli et.al [39]. Ticianelli et.al reported the voltage-current (V-I) curve for a PEMFC for different sets of hydrogen pressure, oxygen pressure and temperature.

However, the values of agglomerate radius, ionomer film thickness and ionomer volume fraction of the PEMFC used in the experimental study was not reported by Ticianelli et.al. Therefore, in this study, we have estimated the value of these parameters using an optimization routine that minimizes the sum of squares error (SSE) between the simulation results and experimental results for one set of operating conditions for one set of operating conditions. The values obtained subsequently were used to solve the model equations and further this model was validated with the experimental results reported by Ticianelli et.al at different set of operating conditions.

4.1 Estimation of unknown parameters

The operational and structural parameters reported by Ticianelli et.al which were used for the estimation of agglomerate radius, ionomer film thickness and ionomer volume fraction are provided in Table 4.1. The values of the physical constants used in the present study are provided in Table 4.2.

The unknown parameters such as agglomerate radius, ionomer film thickness and ionomer volume fraction were estimated using the Matlab function '**fmincon'** which minimizes the objective function as follows:

$$F = \sum_{i=1}^{N} \left(V_{exp} - V_{sim}\right)^2 \tag{4.1}$$

where, V_{exp} and V_{sim} are the experimental and simulated values of the cell voltage respectively. The calculated values of the parameters are reported in Table 4.3.

Table 4.1

Parameter values used for the estimation of agglomerate radius, ionomer film thickness and ionomer volume fraction.

Parameter	**Value**
Temperature	50^0 C
Hydrogen pressure (P_{H_2})	1 atm
Oxygen pressure(P_{O_2})	1 atm
Platinum loading	0.35 mg/cm^2
Pt/C ratio (f)	0.1
CL thickness	50 µm
Ohmic resistance	0.35 Ω cm^2

Table 4.2

Physical constants used for the estimation of agglomerate radius, ionomer film thickness and ionomer volume fraction.

Constant	**Value**
Platinum density	21400 kg/m^3
Carbon density	1800 kg/m^3
Cathodic transfer coefficient	1
Anodic transfer coefficient	0.5
Reference oxygen concentration	1.2 mol/m^3
Bulk electronic conductivity	72700 (Ω m)$^{-1}$
Bulk protonic conductivity	17 (Ω m)$^{-1}$

Table 4.3

Calculated values of the parameters.

Parameter	Value
Agglomerate Radius	0.923 μm
Ionomer film thickness	101.6 nm
Ionomer volume fraction	0.51

The estimated values of agglomerate radius, ionomer film thickness and ionomer volume fraction were used to solve the model equations for the set of operating conditions reported in Table 4.1. The results were obtained for current densities of 0.02, 0.05, 0.1, 0.2, 0.3, 0.4, 0.5 and 0.6 A/cm^2 respectively. The difference between the experimental results and model results is presented in Fig. 4.1. The percentage error between the experimental results and model results is shown in Table 4.4. It can be observed from Table 4.4 that the percentage error varies between 2.8% to 7.7 %. The maximum error is obtained at the highest current density. The coefficient of determination (R^2) is greater than 0.95. This implies that the present model is a good fit to the experimental results.

It can be observed from Fig 4.1 that the cell voltage decreases with increase in current density. The cell voltage decreases very rapidly until the current density reaches 0.1 A/cm^2. The cell potential decreases slowly in a nearly linear fashion for current densities between 0.1 A/cm^2 and 0.4 A/cm^2. The cell voltage then drops more rapidly between 0.4 A/cm^2 and 0.6 A/cm^2. Therefore, the entire V-I curve consist of three regions as discussed in section 1.7. The activation losses are significant in the first region of the V-I curve. The ohmic losses and concentration losses are dominant in the second and third region respectively.

Table 4.4

Comparison between experimental results and model results for T=50^{0}C, P_{H_2}=1 atm, P_{O_2}=1 atm.

Current density (A/cm^2)	V_{exp} (V)	V_{sim} (V)	% Error
0.0005	NA	0.956	NA
0.005	NA	0.890	NA
0.02	0.82	0.844	2.927
0.05	0.782	0.805	2.941
0.1	0.728	0.761	4.533
0.2	0.659	0.689	4.552
0.3	0.597	0.62	3.853
0.4	0.532	0.547	2.820
0.5	0.453	0.466	2.870
0.6	0.364	0.336	7.692
R^2 = 0.9561			

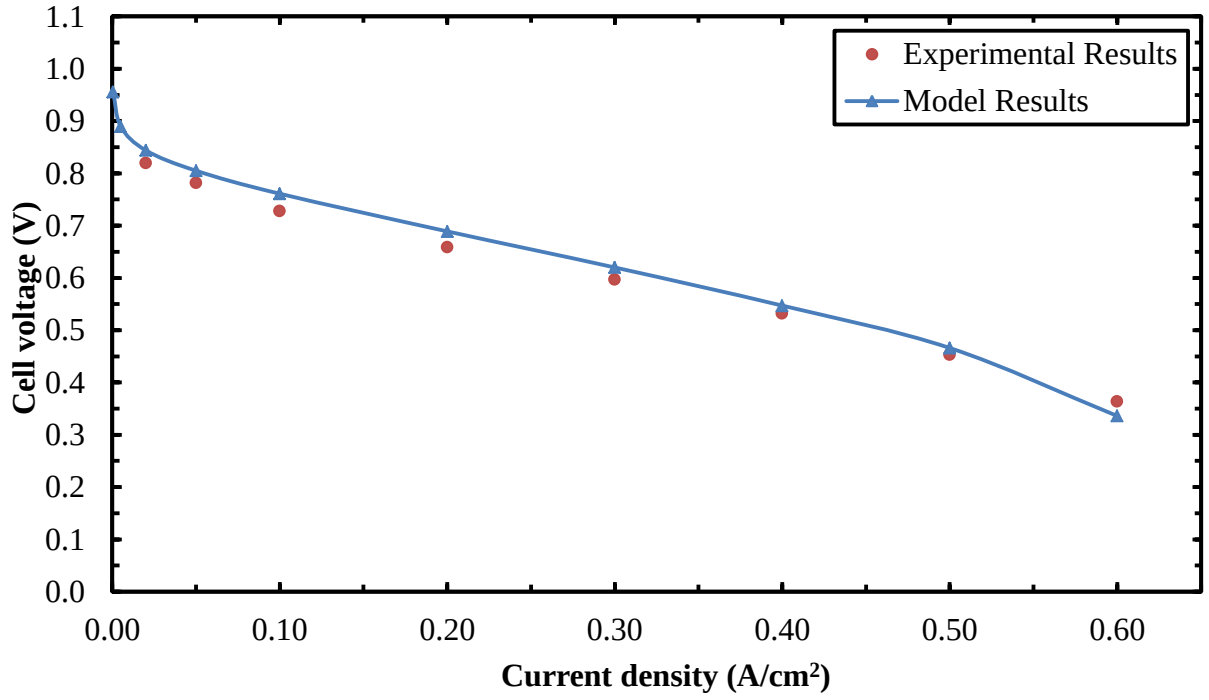

Fig. 4.1. Comparison between experimental results and model results for T=50^{0}C, P_{H_2}=1 atm, P_{O_2}=1 atm.

4.2 Validation of the model

The estimated unknown parameters were used to solve the model equations and the results obtained were validated against the experimental results reported by Ticianelli et.al for the set of operating conditions provided in Table 4.5.

Table 4.5

Operational parameters used for validation of the model.

Parameter	Value
Temperature	80^0 C
Hydrogen pressure	3 atm
Oxygen pressure	5 atm

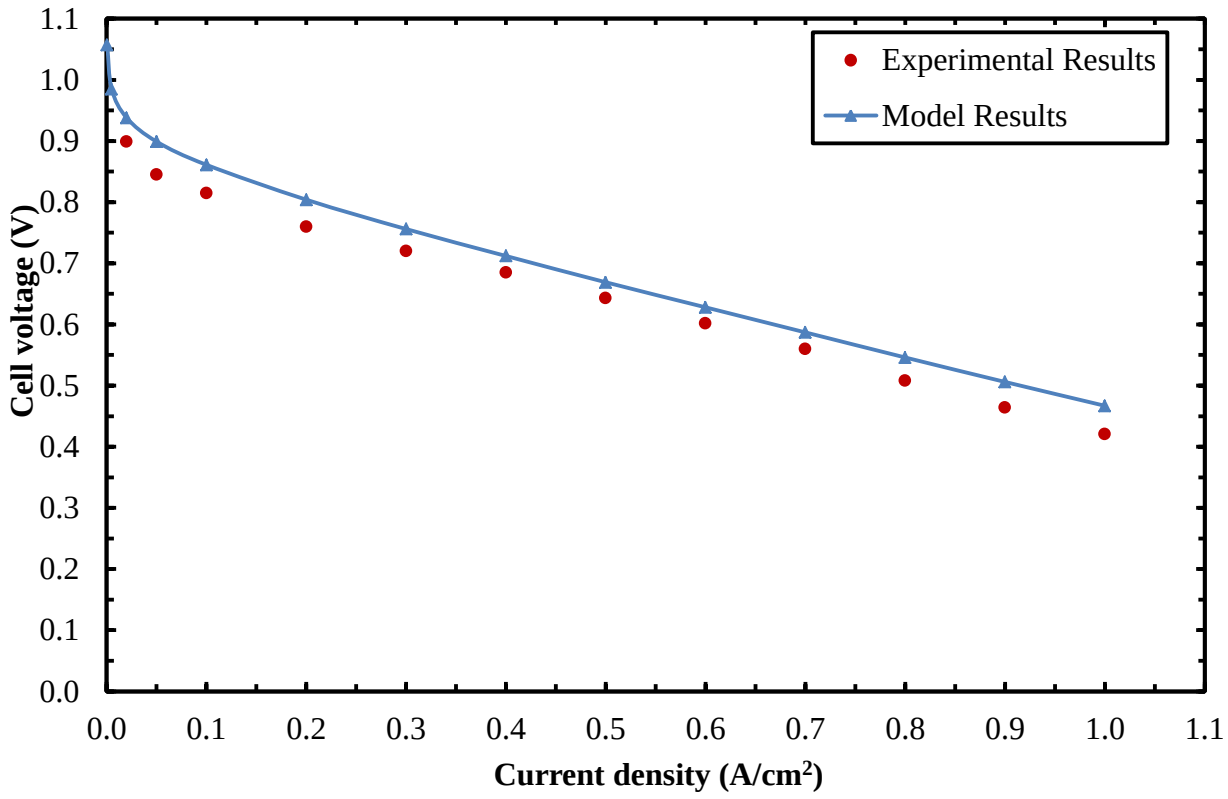

Fig 4.2. Comparison between experimental results and model results for T=80^0C, P_{H_2}=3 atm, P_{O_2}=5 atm.

Table 4.6

Comparison between experimental results and model results for T=80^{0}C, P_{H_2}=3 atm, P_{O_2}=5 atm.

Current density (A/cm^2)	V_{exp} (V)	V_{sim} (V)	% Error
0.0005	NA	1.057	NA
0.005	NA	0.985	NA
0.02	0.899	0.938	4.338
0.05	0.845	0.899	6.390
0.1	0.815	0.861	5.644
0.2	0.76	0.804	5.789
0.3	0.72	0.756	5.000
0.4	0.685	0.712	3.942
0.5	0.643	0.669	4.044
0.6	0.602	0.628	4.319
0.7	0.56	0.587	4.821
0.8	0.508	0.546	7.480
0.9	0.464	0.506	9.052
1	0.421	0.467	10.926

The comparison between the experimental results and the model is presented in Fig. 4.2 and Table 4.6 respectively. It can be observed from Table 4.6 shows that the percentage error varies in the range of 4-11%. The maximum error of 11% is obtained for the highest current density. Hence, the model agrees reasonably well with the experimental data.

It can be observed from Fig 4.2 that the increase in current density leads to a decrease in cell voltage. Initially, the decrease in cell voltage is very steep until the current density reaches 0.1 A/cm^2. For current density greater than 0.1 A/cm^2, the cell potential decreases slowly in a nearly linear fashion.

4.3 Comparison of agglomerate model with pseudo-homogenous model

The pseudo-homogenous model developed in section 3.9 was solved for the set of operating conditions reported in Table 4.5. The results obtained by solving the model equations were compared with the agglomerate model for the same set of operating conditions.

The comparison between the two models is presented in Fig. 4.3. At low current densities, the results calculated using a pseudo-homogenous model is close to the results predicted by the agglomerate model. However, the difference of cell voltage predicted by these two models becomes larger with increase in current density. The cell voltage predicted by the pseudo-homogenous model is always greater than the agglomerate model. This result implies that a pseudo-homogenous model leads to over prediction of cell voltage for the same value of current density. This over prediction in cell voltage is due to the fact that a homogenous model does not take the mass transfer limitations of oxygen into account. These mass transfer limitations are due to dissolution of oxygen into the ionomer film and subsequent to the reaction sites. Also, it can be observed from Fig. 4.3 that the cell voltage initially decreases rapidly and then decreases slowly in a nearly linear manner for pseudo-homogenous model. Since the third region is absent in the V-I curve of a pseudo-homogenous model, it can be concluded that this model does not take the concentration losses into account.

The difference between the voltages predicted by the two models was found to be very less at low current densities. This is because the reaction kinetics is the limiting step at low current densities. But the mass transfer limitations of oxygen become more significant than reaction kinetics at high current densities. The difference between the predictions of the two models was found to increase with increase in current density because oxygen mass transfer limitations were not considered in the pseudo-homogenous model.

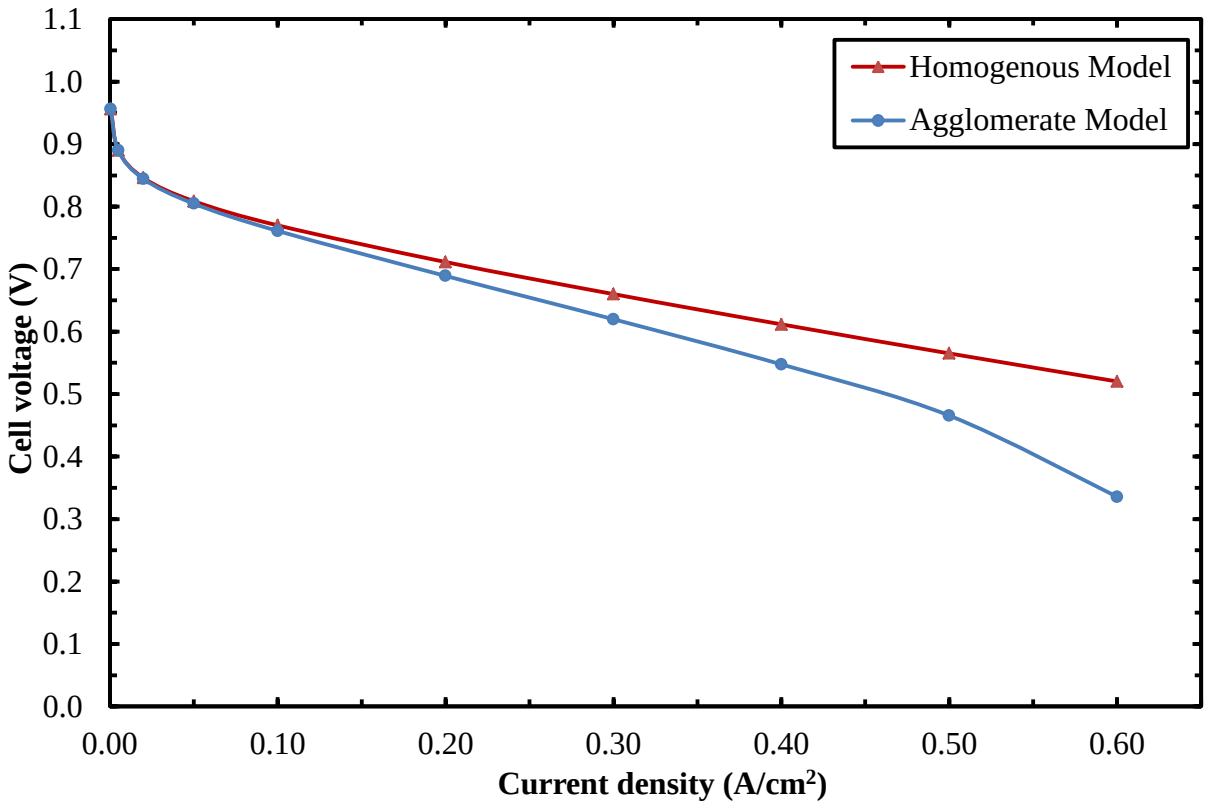

Fig 4.3. Comparison of agglomerate model with pseudo-homogenous model.

4.4 Effect of various parameters

The effect of following parameters was studied and discussed in this section.

1. Temperature
2. Pressure
3. Agglomerate radius
4. Ionomer film thickness
5. Platinum loading
6. Ionomer volume fraction
7. CL thickness

4.4.1 Effect of temperature

To study the effect of temperature on the PEMFC performance, the model equations were solved for 50, 60 and 80^{o}C respectively. The values of other parameters were taken from Table 4.1 and Table 4.3. The effect of temperature on the V-I curve is graphically shown in Fig 4.4.

As seen from Fig.4.4, the cell voltage for the same value of current density increases with increase in temperature. Therefore, the performance of the PEMFC is always improved with increase in temperature. This is because the performance of PEMFC cathode is primarily determined by reaction kinetics and mass transfer of oxygen. An increase in temperature improves the kinetics of electrochemical reactions. The bulk diffusivity of oxygen also increases with temperature. However, a PEMFC normally operates between 40-100^{o}C. If temperature of the cell is increased beyond 100^{o}C, the membrane starts to dry out which decreases proton conductivity and hence increases the ohmic losses of the cell. This puts a physical limit to the operating temperature of PEMFC. It can also be observed from Fig. 4.4 that the relative increase in cell voltage decreases with increase in operating temperature.

4.4.2 Effect of oxygen pressure

To study the effect of oxygen pressure on the V-I curve, the model equations were for oxygen pressure of 1, 3 and 5 atm respectively. The values of other parameters were taken from Table 4.1 and Table 4.3. The V-I curve for these three temperature conditions is shown in Fig. 4.5.

It can be observed from Fig. 4.5 that the cell voltage increases with increase in pressure for the same value of current density. Therefore, an increase in oxygen pressure always improves the performance of PEMFC. This is because oxygen acts as a reactant in the electrochemical reaction in the cathodic half-cell. So, an increase in pressure of oxygen increases the rate of reaction. Higher reaction rate leads to higher current densities and lower polarization losses. The reversible cell potential also increases with pressure. Both these factors improve the performance of PEMFC.

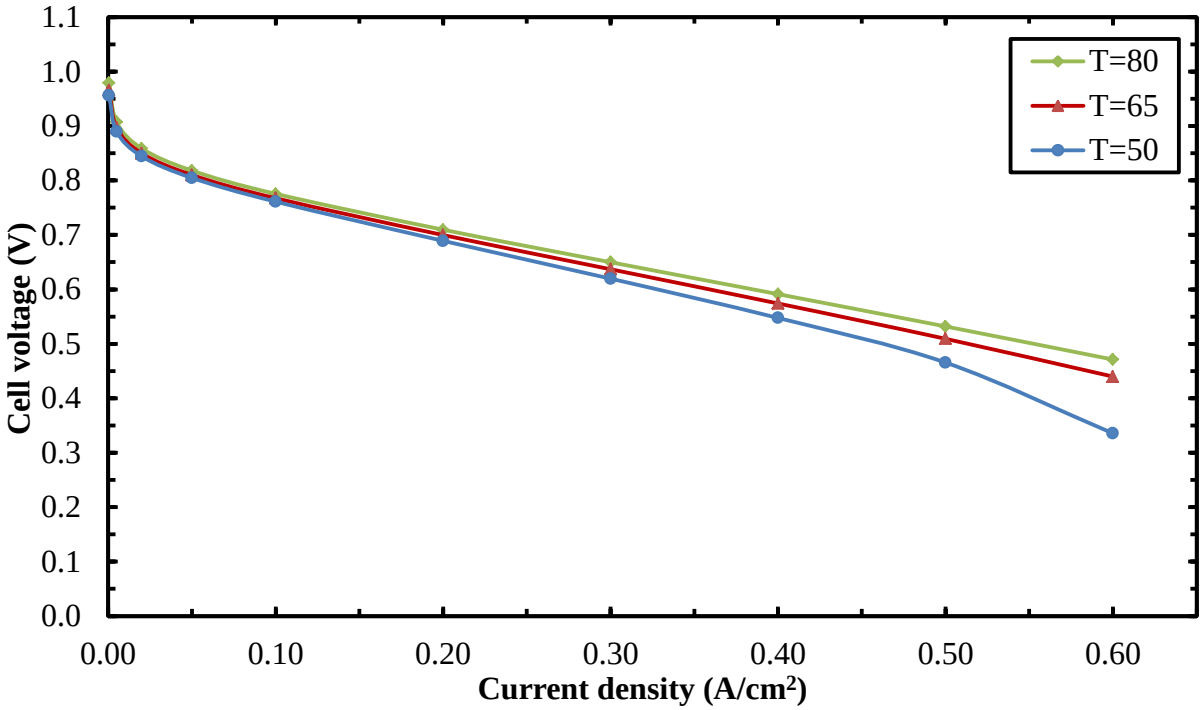

Fig 4.4. Effect of temperature on PEMFC performance.

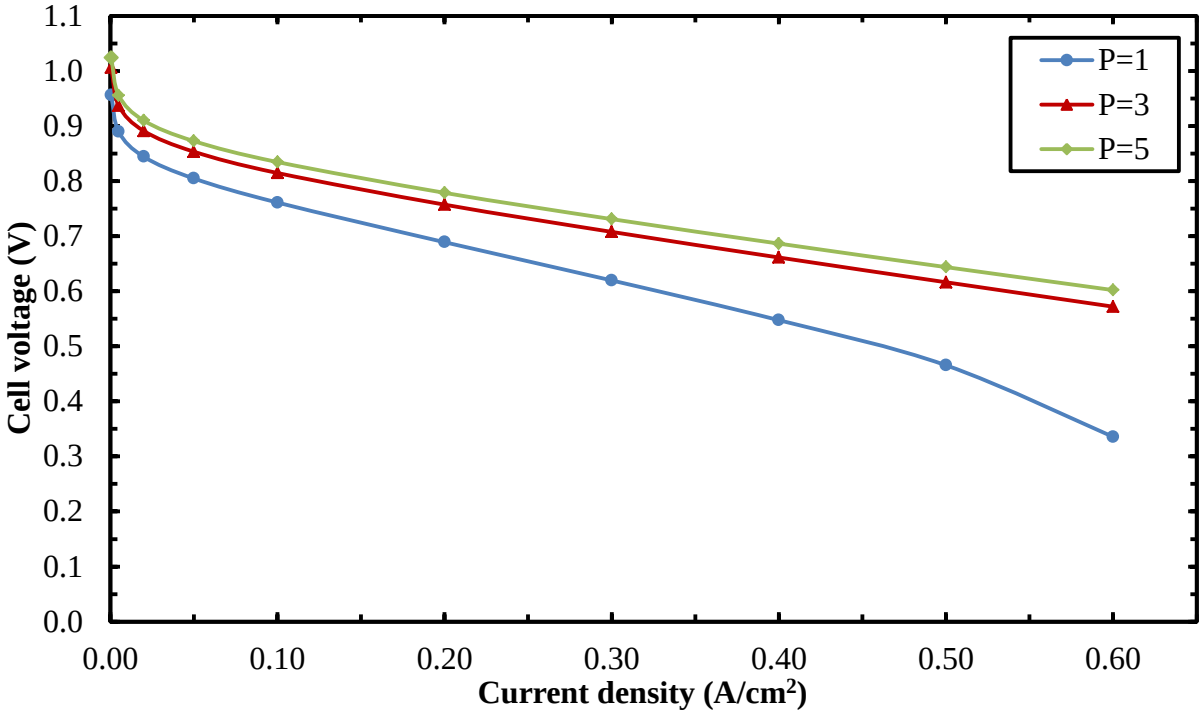

Fig 4.5. Effect of oxygen pressure on PEMFC performance.

4.4.3 Effect of agglomerate radius

To study the effect of agglomerate radius on V-I curve, the model equations were solved for agglomerate radii of 0.4, 0.6, 0.923, 1.3 and 1.5 μm respectively. The values of other parameters were taken from Table 4.1 and Table 4.3. The effect of agglomerate radius on V-I curve is presented in Fig. 4.6.

It can be observed from Fig. 4.6 that an increase in agglomerate radius shifts the V-I curve downwards. This is due to the reason that larger agglomerate increases the diffusive path travelled by oxygen to reach the reaction sites. Therefore, it increases the mass transfer resistance of oxygen. Another reason is that an increase in agglomerate size decreases the area available of dissolution of oxygen in the nafion film, (a_{agg}). This result implies that an ideal CL should contain agglomerates of very small sizes. However, regulating the size of agglomerates in the preparation of CL remains as one of the main challenges of modern PEMFC technology.

Similar results were reported by Kamarajugadda and Majumdar [28]. They studied the effect of agglomerate radius on the performance of PEMFC based on an agglomerate model for the CCL. The model was simulated for agglomerate radius of 0.05, 0.1, 0.2, 0.6 and 1 μm respectively. The CL thickness, Pt/C ratio, platinum loading, ionomer fraction and ionomer film thickness were kept as 15 μm, 0.28, 0.45 mg/cm^2, 0.4 and 100 nm respectively. On comparing of the V-I curve for five agglomerate radii showed, it was observed that the performance of PEMFC improved with decrease in agglomerate radius.

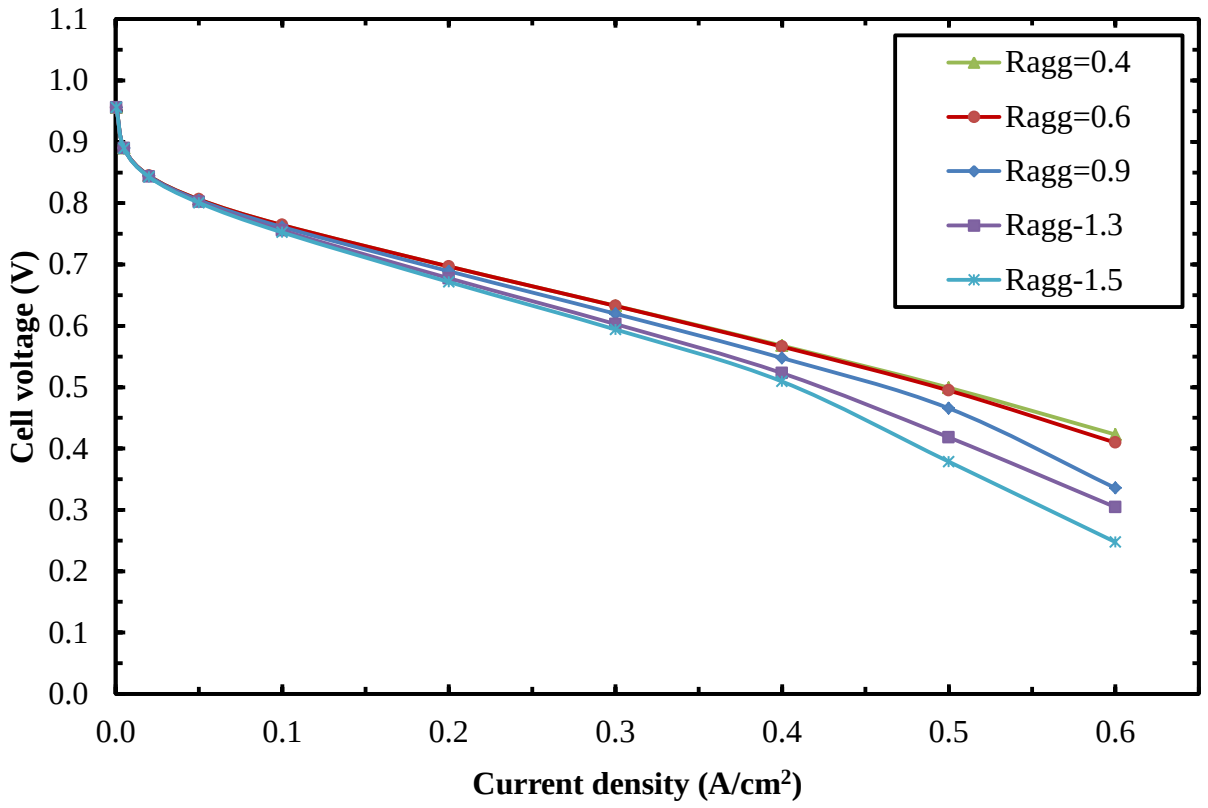

Fig 4.6. Effect of agglomerate radius on PEMFC performance.

4.4.4 Effect of ionomer film thickness

To study the effect of ionomer film thickness on V-I curve, the model equations were solved for ionomer film thickness of 60, 80, 101.6, 120 and 140 nm respectively. The values of other parameters were taken from Table 4.1 and Table 4.3. The effect of ionomer film thickness on V-I curve is presented in Fig. 4.6.

It can be seen from Fig 4.7 that a decrease in ionomer film thickness improves the performance of PEMFC. This is because the diffusion path of oxygen becomes shorter for a thinner ionomer film. This decreases the mass transfer resistance of oxygen in the CL. The area available for dissolution of oxygen in the nafion film(a_{agg}) also increases with the decrease in ionomer film thickness. Therefore, an ideal CL should contain agglomerates with very thin ionomer films. However, the ionomer film provides a continuous path for the flow of protons. So, the ionomer film could not be completely eliminated in the design of CCL.

Similar results were reported by Secanell et.al [19]. Secanell et.al developed an agglomerate model for the PEMFC to calculate the optimum values of different parameters of the CCL. The model was solved for ionomer film thickness of 0, 40 and 80 nm respectively. The current density for the three cases was found to be 1.6, 1.16 and 0.944 A/cm^2 respectively.

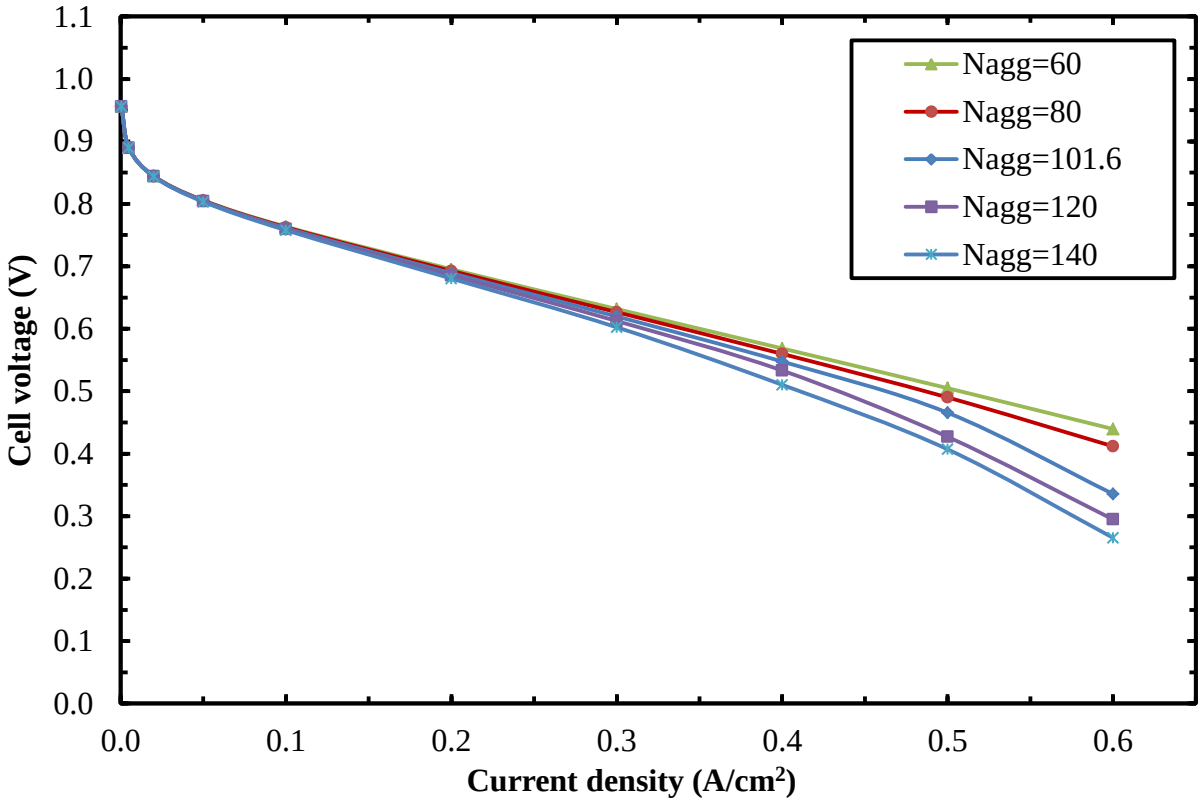

Fig 4.7. Effect of ionomer film thickness on PEMFC performance.

4.4.5 Effect of platinum loading

The effect of platinum loading on PEMFC performance was studied by solving the model equations for overpotential of 0.3 V, 0.6 V and 0.9 V respectively. Platinum loading was varied from 0.15-1.05 mg/cm^2 for the first case, 0.25-0.75 mg/cm^2 for the second case and 0.15-0.65 mg/cm^2 for the third case respectively with a step size of 0.1 mg/cm^2. The values of other parameters were taken from Table 4.1 and Table 4.3. Variation of current densities with platinum loading for the three cases is presented in Figs. 4.8, 4.9 and 4.10.

As shown in Figs. 4.8, 4.9 and 4.10, the current density first increases with increase in platinum loading, reaches a maximum value and then decreases. The platinum loading at which maximum current density is obtained is the optimum platinum loading. The optimum platinum loading for overpotential of 0.3, 0.6 and 0.9 V was found to be 0.9, 0.5 and 0.35 mg/cm^2 respectively. The current densities at optimum platinum loading were found to be 0.17, 0.35 and 0.98 respectively. Comparison of the three figures also show that the optimum platinum loading decreases with increase in activation overpotential.

An increase in platinum loading leads to two competing effects on PEMFC performance.

1. It increases the active area for electrochemical reactions and therefore improves the performance of PEMFC.
2. Since the Pt/C ratio is kept constant, the carbon loading increases with increase in platinum loading. This increase in carbon loading reduces the porosity of the CL. The reduced porosity increases the mass transfer resistance of oxygen. This has a negative impact on PEMFC performance.

An analysis of these two effects suggest that an optimum platinum loading should exist that maximizes current density. For this reason, an optimum value of platinum loading was obtained for all three cases which were studied.

The current density of PEMFC increases with increase in activation overpotential. Therefore, low overpotential implies low current density and high overpotential implies high current density. At low current density, the performance of PEMFC is limited by rate of electrochemical reaction. The mass transfer limitations for oxygen are not significant in these conditions. So, a higher platinum loading is required to maximize current since higher loading increase the rate of electrochemical reaction. However, mass transfer resistance of oxygen becomes more important than the kinetic rate with increase in current density. For this reason, the optimum platinum loading decreases from 0.9 to 0.35 mg/cm^2 with increase in overpotential from 0.3 to 0.9 V.

Similar results were reported by Srinivasarao et.al [40]. Srinivasarao et.al obtained the optimum values of platinum loading for different overpotentials. The optimum platinum loading for overpotential of 0.8, 0.9 and 1 V were found to be 0.39, 0.35 and 0.335 respectively.

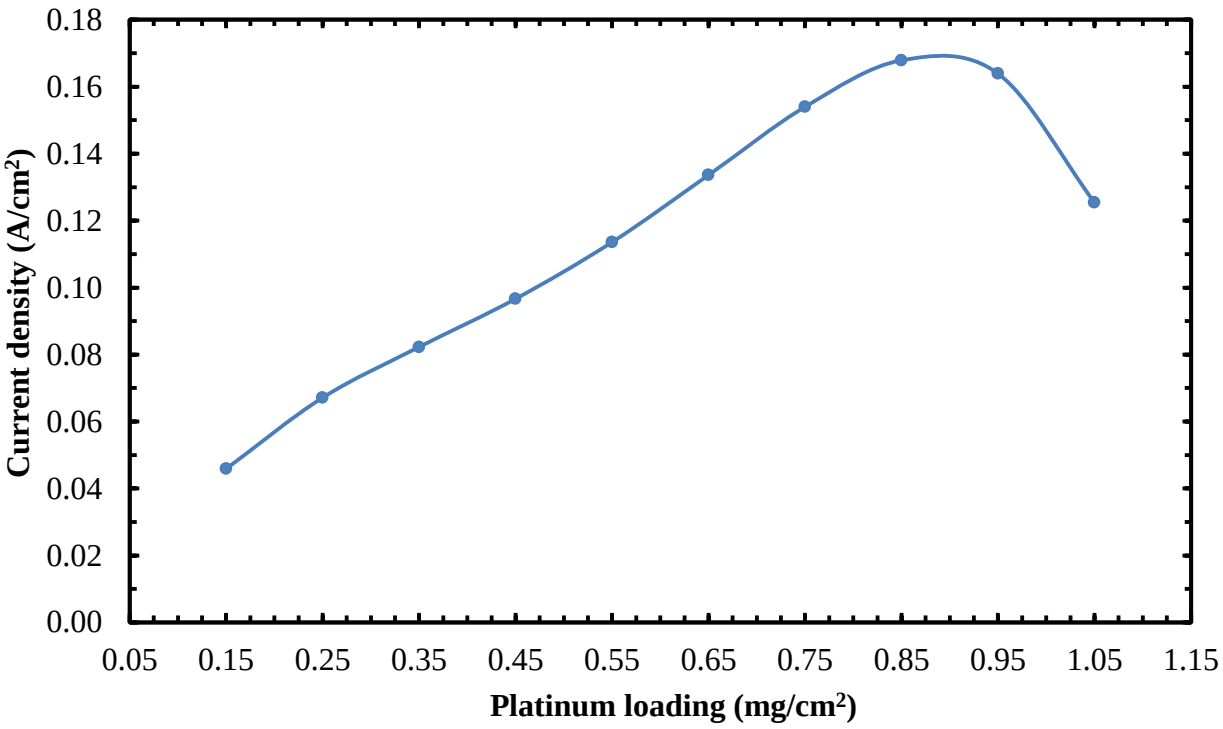

Fig. 4.8. Variation of current density with platinum loading for overpotential of 0.3 V.

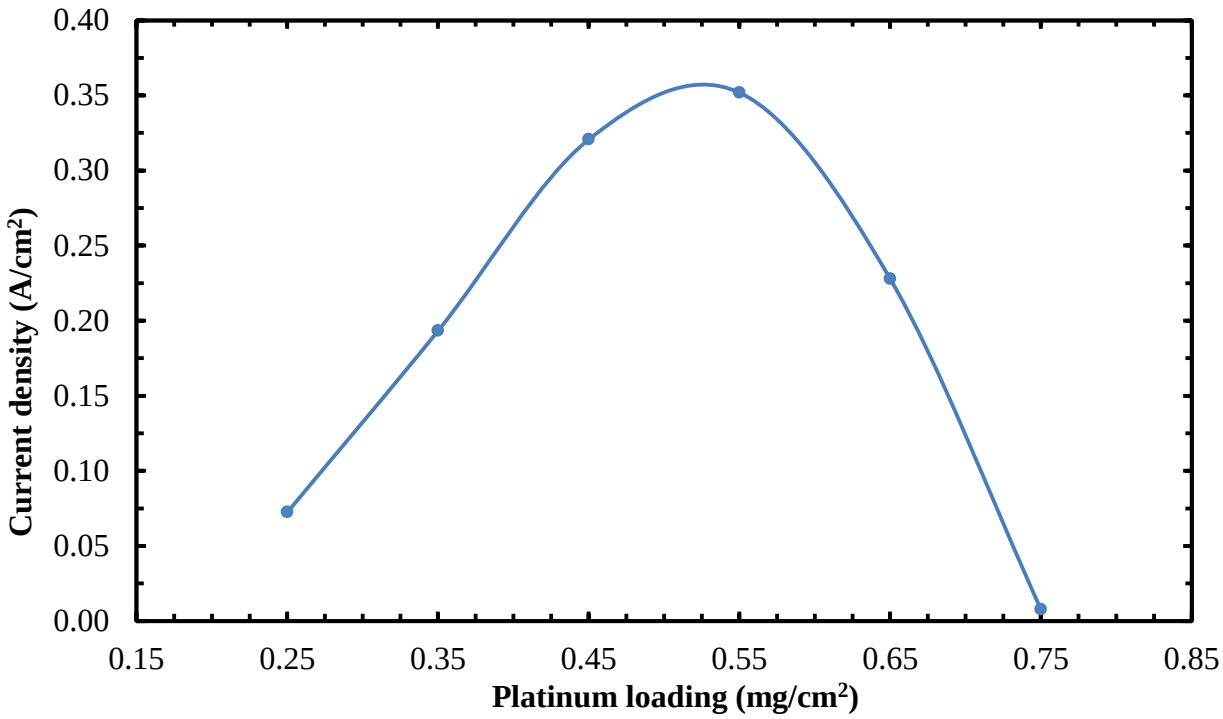

Fig. 4.9. Variation of current density with platinum loading for overpotential of 0.6 V.

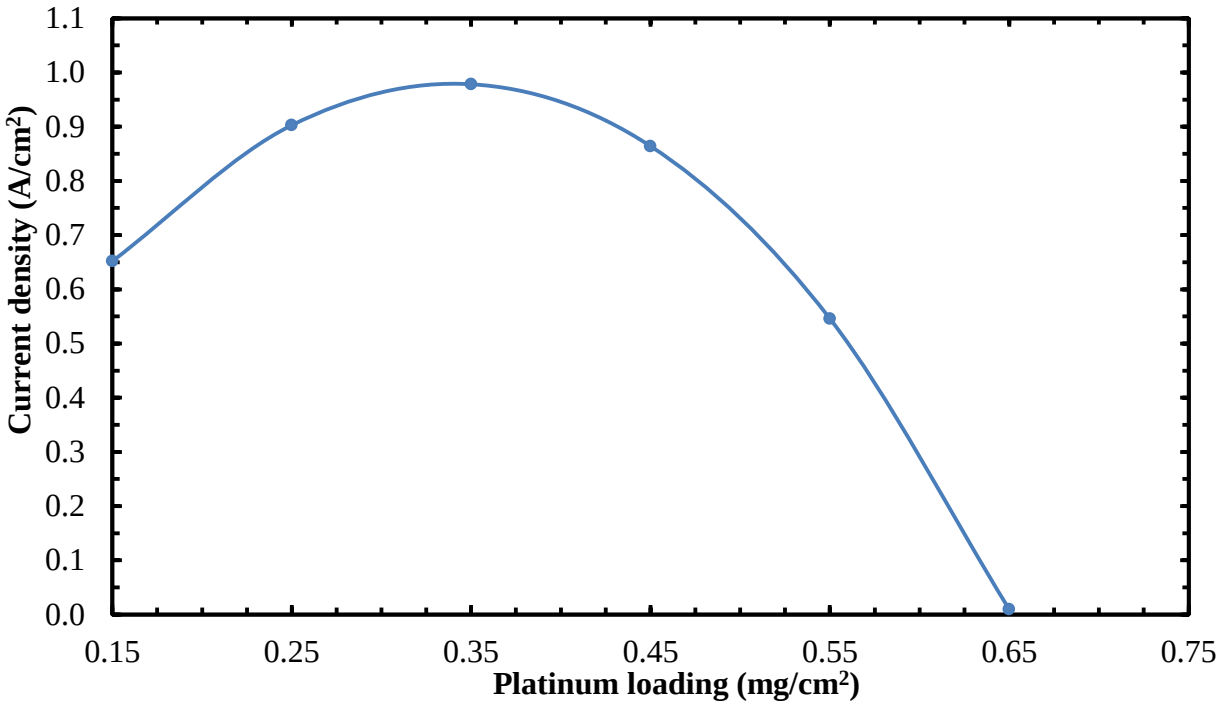

Fig. 4.10. Variation of current density with platinum loading for overpotential of 0.9 V.

4.4.6 Effect of ionomer volume fraction

The effect of ionomer volume fraction on the performance of PEMFC was studied by solving the model equations for overpotential of 0.3 V, 0.6 V and 0.9 V respectively. Ionomer volume fraction was varied from 0.15 to 0.75 with a step size of 0.1. The values of other parameters were taken from Table 4.1 and Table 4.3. Variation of current densities with ionomer volume fraction for the three cases is presented in Figs. 4.11, 4.12 and 4.13.

It can be observed from Figs. 4.11, 4.12 and 4.13 that the current density first increases with increase in ionomer volume fraction, reaches a maximum value and then decreases. The ionomer volume fraction at which maximum current density is obtained is the optimum ionomer fraction. The optimum ionomer volume fraction for overpotential of 0.3, 0.6 and 0.9 V was found to be 0.3, 0.35 and 0.55 respectively. The current densities at optimum ionomer volume fraction were found to be 0.11, 0.61 and 0.86 respectively. Comparison of the three figures also show that the optimum ionomer fraction increases with increase in activation overpotential. This is opposite to the behavior of optimum platinum loading with change in overpotential.

Similar to the effect of platinum loading on PEMFC performance, an increase in ionomer volume fraction leads to two competing effects:

1. Increase in ionomer volume fraction decreases the CL porosity. Hence, it increases the mass transport resistance of oxygen reaching the reaction sites. This negatively influences the performance of PEMFC.
2. Increase in ionomer volume fraction decreases the voltage losses due to proton transport. It also increases the number of agglomerates per unit volume (n_{agg}) according to equation (3.98). The effective area of agglomerates available for dissolution of oxygen into the ionomer film(a_{agg}) is directly proportional to n_{agg} .Therefore, increase n_{agg} leads to increase in a_{agg}. This increase in a_{agg} improves the performance of the PEMFC.

Due to these two competing effects, an optimum value of ionomer volume fraction was obtained for all three cases which were studied. Also, the effect of a_{agg} becomes more significant at high current densities. For this reason, the optimum value of ionomer volume fraction increases from 0.3 to 0.55 with increase in overpotential from 0.3 to 0.9 V.

Earlier studies done by Song et.al [17] and Sun et.al [30] reported the optimum value of ionomer film thickness for overpotentials of 0.6 and 0.5 V respectively. The effect of overpotential of optimum ionomer fraction was not considered in their studies. Therefore, the present study is an improvement upon the earlier studies as it has taken the effect of overpotential on optimum ionomer volume fraction into account and also provided an explanation for this effect.

4.4.7 Effect of CL thickness

To analyze the effect of CL thickness on PEMFC performance, the variation of current density, oxygen concentration and activation overpotential with distance from the CL /GDL interface was calculated for the base case conditions reported in Table 4.1 and 4.3. These variations were calculated in terms of normalized distance, normalized current, normalized oxygen concentration and normalized overpotential.

Normalized distance = $\frac{x}{l_c}$

Normalized current = $\frac{i}{I}$

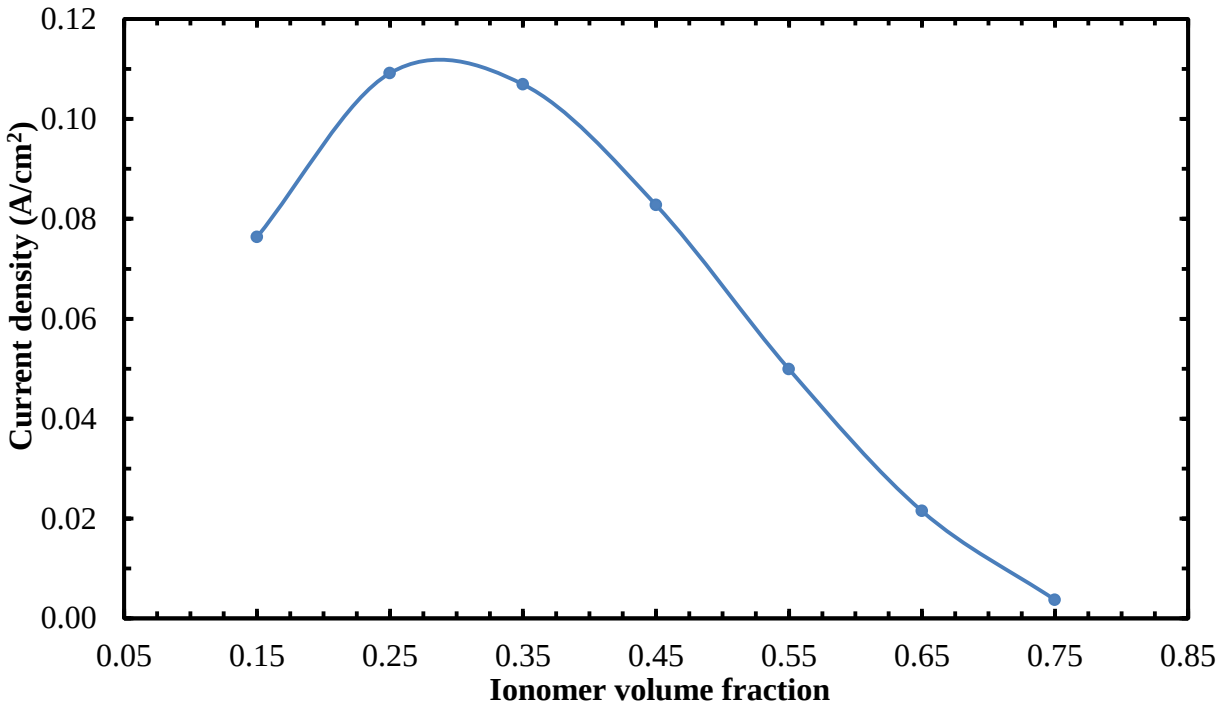

Fig. 4.11. Variation of current density with ionomer volume fraction for overpotential of 0.3 V.

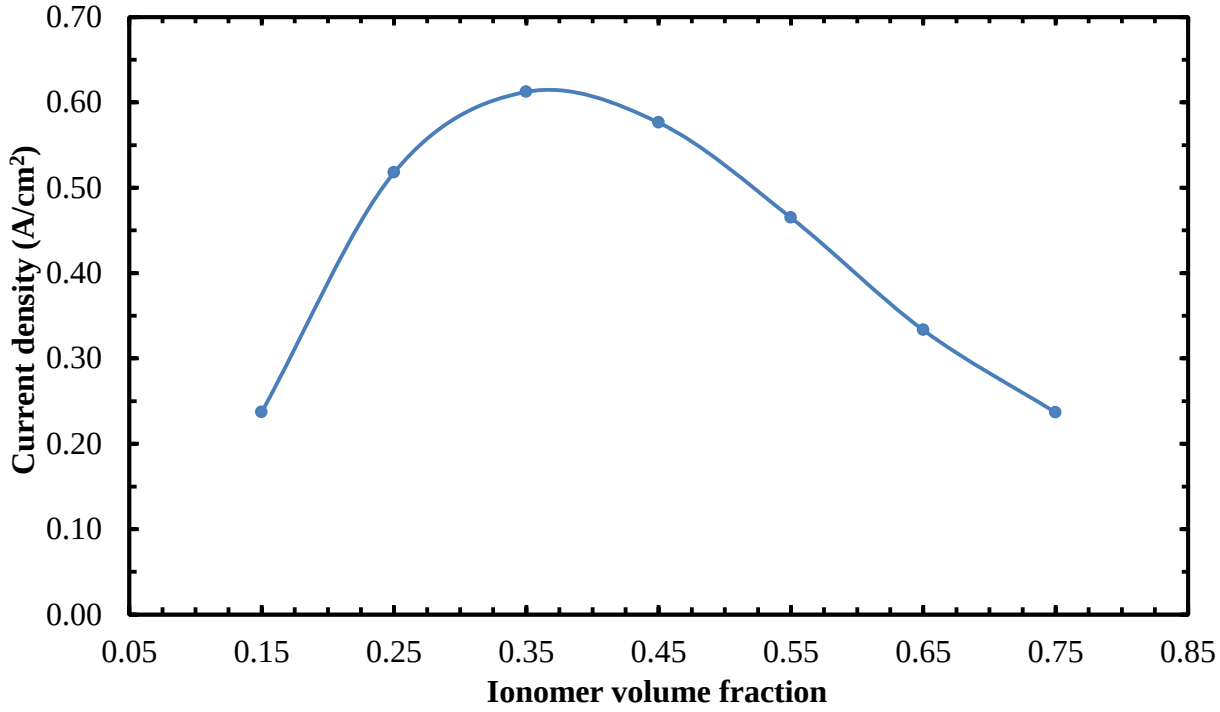

Fig. 4.12. Variation of current density with ionomer volume fraction for overpotential of 0.6 V.

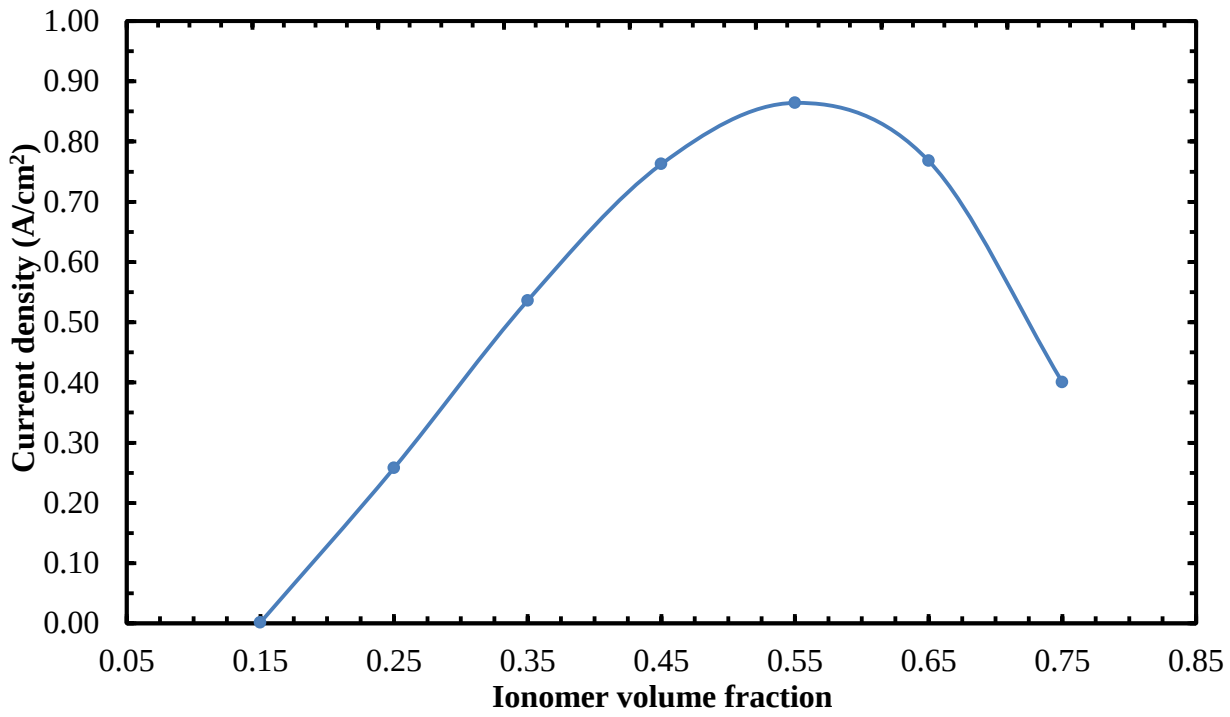

Fig. 4.13. Variation of current density with ionomer volume fraction for overpotential of 0.9 V.

Normalized oxygen concentration = $\frac{C_{O_2}}{C_{O_2}\ at\ l=l_c}$

Normalized overpotential = $\frac{\eta}{\eta\ at\ l=l_c}$

The variation of current, oxygen concentration and overpotential with distance is shown in Figs 4.14, 4.15 and 4.16 respectively. It can be seen from Fig 4.14 that the protonic current density increases rapidly up to 60% of the total CL thickness. It then increases slowly and finally saturates to a value of *I* when the normalized distance reaches 0.9. Similarly, the oxygen concentration initially shows a rapid decline and then almost reduces to zero when the normalized distance becomes 0.9. It can also be observed from the Fig. 4.15 that 97% of oxygen is consumed to generate electric current within a normalized distance of 0.6. Therefore, the rest of the CL remains nearly unused and can be termed as dead catalyst region. Also, it is observed from Fig. 4.16 that the activation overpotential remains nearly unchanged with the distance.

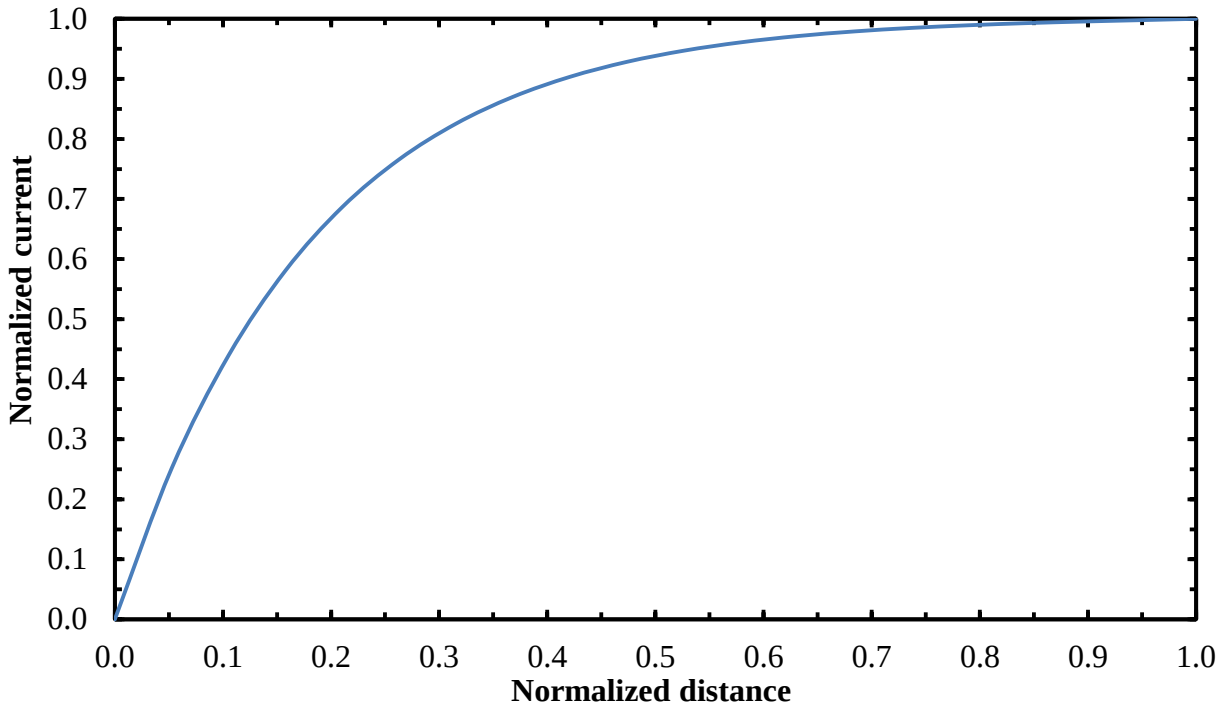

Fig. 4.14. Variation of current with distance from the CL-GDL interface.

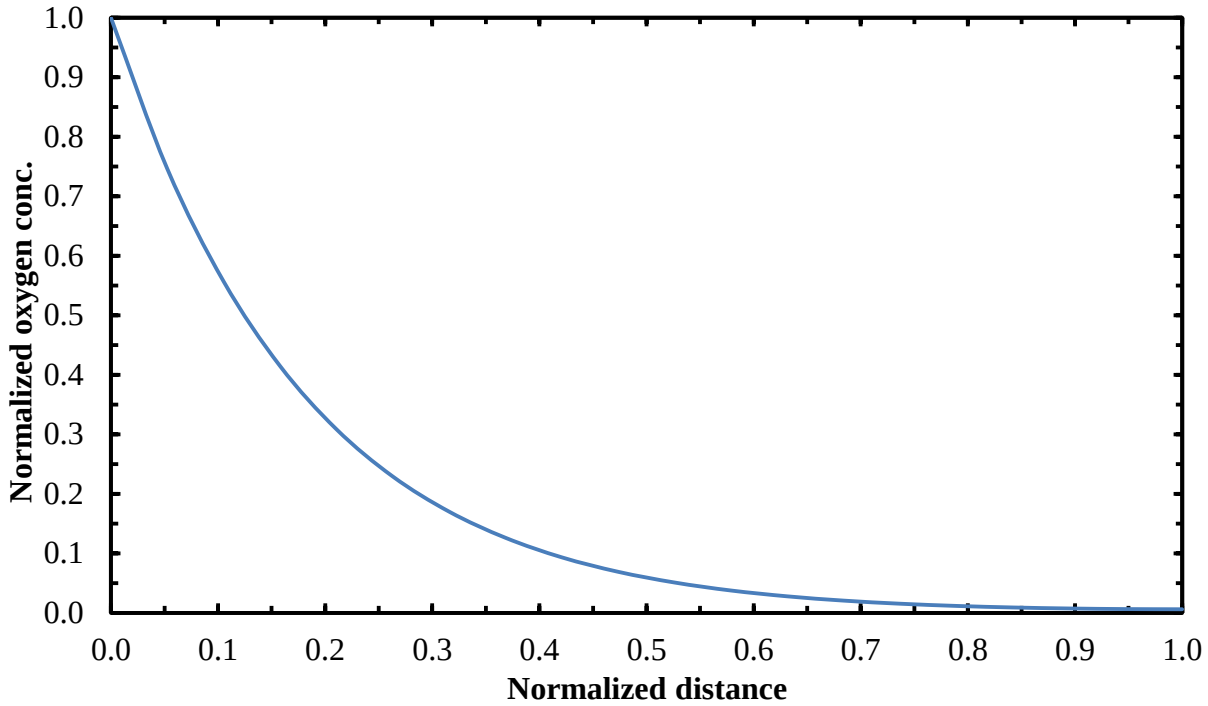

Fig. 4.15. Variation of oxygen concentration with distance from the CL-GDL interface.

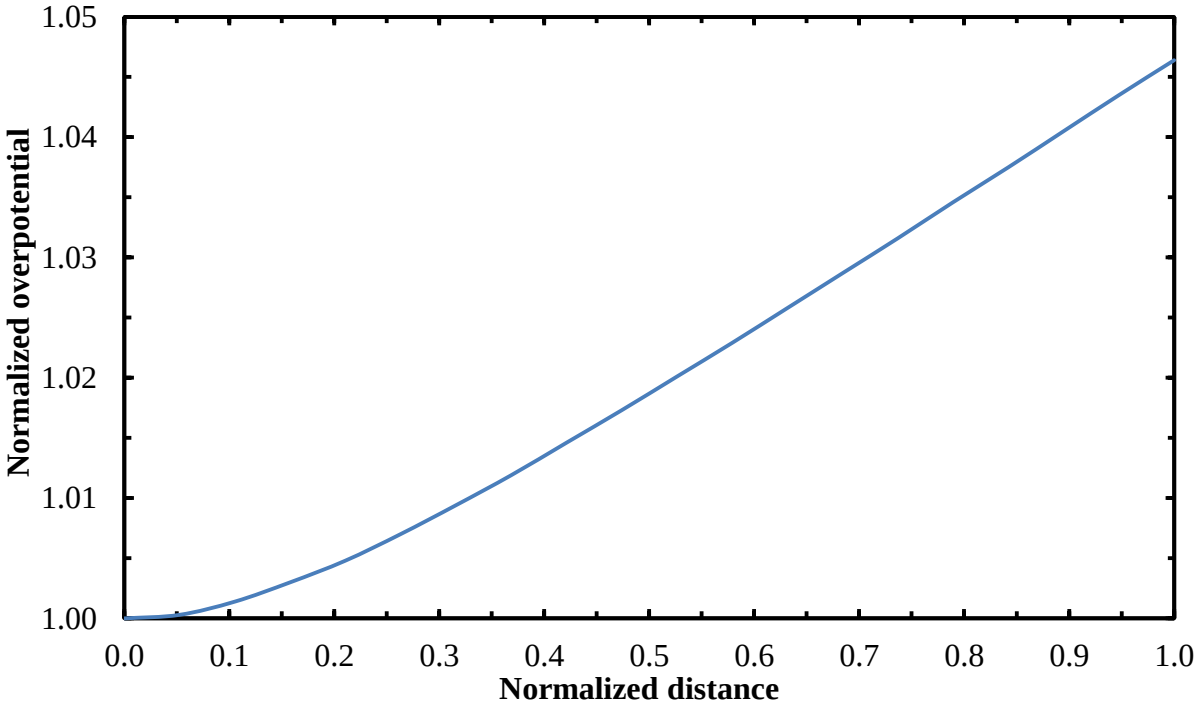

Fig. 4.16. Variation of overpotential with distance from the CL-GDL interface.

Since 40% of the catalyst region remains unused, it can be concluded that a thinner CL leads to better utilization of the platinum catalyst. To verify this conclusion, the variation of current density with distance from the CL-GDL interface for three values of CL thickness- 50, 70 and 90 μm was calculated by solving the model equations. The results are presented in Fig. 4.17.

It can be observed from Fig. 4.17 that the distance at which the current density reaches the saturation value decreases with the increase in CL thickness. This result implies that the utilization of the catalyst decreases with increase in CL thickness. Therefore, future efforts in PEMFC technology should be directed at developing thinner catalyst layers which improve the utilization of platinum.

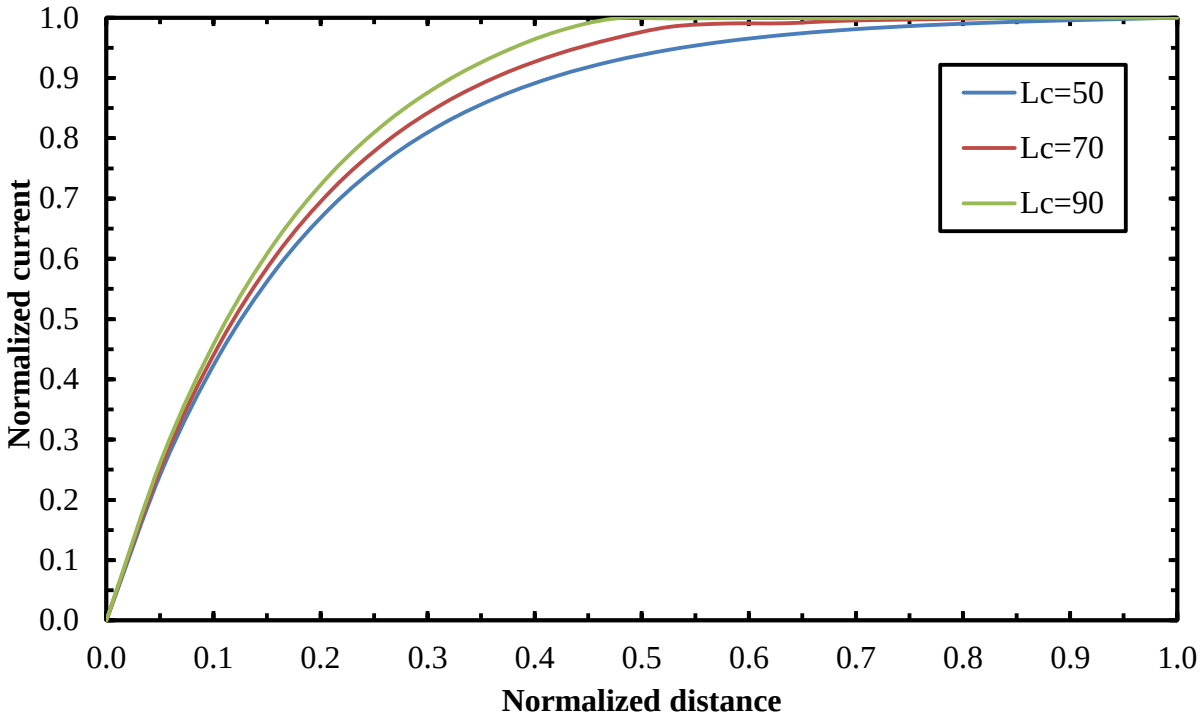

Fig. 4.17. Effect of CL thickness on current density profile inside the CL.

CHAPTER-5
CONCLUSIONS AND RECOMMENDATIONS

5.1 Conclusions

In this study, a mathematical model was developed for the CCL of a PEMFC using a comprehensive agglomerate model. The present model can be reduced to a pseudo-homogenous model when the agglomerate radius approaches zero. The model was validated against the experimental data reported by Ticianelli et.al. The agglomerate model was compared with the pseudo-homogenous model. The effect of various parameters such as operating temperature, oxygen pressure, agglomerate radius, ionomer film thickness, platinum loading, ionomer volume fraction and CL thickness on the performance of PEMFC cathode was studied. The conclusions drawn from these studies are as follows:

1. The pseudo-homogenous model was found to over predict the current density as compared to the agglomerate model. The difference in current densities predicted by the two models became larger with increase in cell voltage. This is because the pseudo-homogenous model fails to account for the mass transfer limitations of oxygen.
2. The performance of PEMFC cathode was found to improve with increase in temperature due to the enhanced reaction rate and increased diffusivity of oxygen at higher temperatures.
3. Increase in oxygen pressure was observed to improve the PEMFC performance. The reason is that the both the reversible cell potential and electrochemical reaction rate increases with increase in oxygen pressure.
4. Increase in agglomerate radius and ionomer film thickness was observed to have a negative influence on PEMFC performance. This decrease in performance could be attributed to the fact that both the increase in agglomerate radius and ionomer film thickness increase the mass transfer resistance of oxygen and decreases the area available for dissolution of oxygen.
5. The optimum platinum loading at overpotential of 0.3, 0.6 and 0.9 V were found to be 0.9, 0.5 and 0.35 mg/cm^2 respectively. Increase in platinum loading enhances the reaction rate but increases mass transfer resistance of oxygen. The optimum platinum loading decreases with increase in overpotential because the mass transfer limitations become more important than reaction rate at higher current densities.

6. The optimum ionomer volume fraction at overpotential of 0.3, 0.6 and 0.9 V was found to be 0.3, 0.35 and 0.55 respectively. Increase in ionomer fraction increases the area available for dissolution of oxygen but increases the mass transfer resistance of oxygen. The optimum ionomer fraction decreases with increase in overpotential because a_{agg} exerts a greater influence on PEMFC performance at higher current densities.
7. The utilization of the CL was found to decrease with increase in CL thickness.

5.2 Recommendations

1. In this study, we have considered a 1-D steady state model for the CCL. Further studies can be done for two dimensional and dynamic models for the CCL.
2. The liquid saturation of the pores was assumed to be 100% for the present model. The effect of partial saturation of the pores could be studied.
3. A rigorous optimization can be done that take all the operational and structural parameters simultaneously into account.

REFERENCES

1. http://en.wikipedia.org/wiki/Proton_exchange_membrane_fuel_cell.
2. J.Larminie, A. Dicks, Fuel Cell Systems Explained, John Wiley & Sons, New York, 2003.
3. S. J. Paddison, K. S. Promislaw, Device and Material Modeling in PEM fuel cells, Springer, 2009.
4. N. Wagner, W. Schnurnberger, B. Mueller, M. Lang, Electrochim. Acta 43 (1998) 3785–3793.
5. E.I. Santiago, M.S. Batista, E.M. Assaf, E.A Ticianelli, J. Electrochem. Soc. 151 (2004) 944–947.
6. F. Barbir, PEM Fuel Cells: Theory and Practice, Elsevier Academic Press, 2005.
7. T. Berning, N. Djilali, J. Power Sources 124 (2003) 440-452.
8. W. Tiedemann, J. Newman, J. Electrochem. Soc. 122 (1975) 1482-1485.
9. S.J. Ridge, R.E. White, Y. Tsou, R.N Beaver, G.A Eisman, J. Electrochem. Soc. 136 (1989) 1902-09.
10. M. Wilson, S. Gottesfeld, J. Appl. Electrochem. 22 (1992) 1–7.
11. Y. Rho, S. Srinivasan, Y. Kho, J. Electrochem. Soc. 141(1994) 2089–2096.
12. T.E. Springer, T.A. Zawodzinski, S. Gottesfeld, J. Electrochem. Soc. 138 (1991) 2334-2342.
13. D.M Bernardi, M.W Verbrugge, J. Electrochem. Soc. 139 (1992) 2477-2491.
14. C. Marr, X. Li, J. Power Sources, 77 (1999) 17–27.
15. M. Eikerling, A. Kornyshev, J. Electroanal. Chem. 453 (1998) 89–106.
16. A.A Kulikovsky, Electrocatalysis 3 (2012) 132-138.
17. D. Song, Q. Wang, Z. Liu, T. Navessin, M. Eikerling, S. Holdcroft, J. Power Sources 126 (2004) 104-111.
18. M. Secanell, B. Carnes, A. Suleman, N. Djilali, Electrochim. Acta 52 (2006) 2668-2682.
19. M. Secanell, K. Karan, A. Suleman, N. Djilali, Electrochim. Acta, 52 (2007) 6318-6337.
20. N. Khajeh-Hosseini-Dalasm, M.J. Kermani, D.G. Moghaddam, J.M. Stockie, Int. J. Hydrogen Energy 35 (2010) 2417-2427.
21. R.P. Iczkowski, M.B. Cutlip, J. Electrochem. Soc 127 (1980) 1433-1440.
22. K.Broka, P.Ekdunge, J. Appl. Electrochem. 27 (1997) 281-289.
23. N.P. Siegel, M.W. Ellis, D.J. Nelson, M.R. von Spakovsky, J. Power Sources 115 (2003) 81–89

24. K. Yin, J. Electrochem. Soc. 152 (2005) A583–A593.
25. D. Harvey, J.G. Pharoah, K. Karan, J. Power Sources 179 (2008) 209-219.
26. Q. Wang, M. Eikerling, D. Song, Z. Liu, J. Electroanal. Chem. 573 (2004) 61–69.
27. Q. Wang, D. Song, T. Navessin, S. Holdcroft, Z. Liu, Electrochim. Acta 50 (2004) 725-730.
28. S. Kamarajugadda, S. Mazumder, J. Power Sources 183 (2008) 629–642.
29. S. Kamarajugadda, S. Mazumder, J. Power Sources 208 (2012) 328–339.
30. W. Sun, B.A. Peppley, K. Karan, Electrochim. Acta, 50 (2005) 3359–3374.
31. W.K Epting, S. Litster, Int. J. Hydrogen Energy 37 (2012) 8505-8511.
32. P.K. Das, X. Li, Z.S. Liu, J. Power Sources 179 (2008) 186-199.
33. N. Khajeh-Hosseini-Dalasm, M. Fesanghary, K. Fushinobua, K. Okazakia, Electrochim. Acta 60 (2012) 55-65.
34. J.C. Amphlett, R.M. Baumert, R.F. Mann, B.A. Peppley, P.R. Roberge, J. Electrochem. Soc. 142 1 (1995) 1–8.
35. A. Parthasarathy, S. Srinivasan, A.J. Appleby, J. Electrochem. Soc. 139 (1992) 2530–2537.
36. R.H. Perry, D.W. Green, Perry's Chemical Engineers' Handbook, McGraw-Hill, New York, 1997.
37. R.B. Bird, W.E. Stewart, E.N. Lightfoot, Transport Phenomena, Wiley, New York, 1960.
38. D.M. Bernardi, M.W. Verbrugge, AIChE J. 37 (1991) 1151-1163.
39. E.A. Ticianelli, C.R. Derouin, A. Redondo, S. Srinivasan, J Electrochem. Soc. 135 (1988) 2209–2214.
40. M. Srinivasarao, D. Bhattacharyya, R. Rengaswamy, S. Narasimhan, Chem. Eng. Res. 89 (2011) 10-22.